FIELD-TESTING OF A PASSIVE SURFACE WATER FLUX METER FOR THE DIRECT MEASUREMENT OF WATER AND SOLUTE MASS FLUXES

By

ERIN C. ATKINSON

A THESIS PRESENTED TO THE GRADUATE SCHOOL
OF THE UNIVERSITY OF FLORIDA IN PARTIAL FULFILLMENT
OF THE REQUIREMENTS FOR THE DEGREE OF
MASTER OF SCIENCE

UNIVERSITY OF FLORIDA

2007

To my parents, who raised three daughters to be strong and intelligent women.

ACKNOWLEDGMENTS

First and foremost, I would like to sincerely thank my advisor, Dr. James W. Jawitz, for his invaluable advice, support, and insight. His active involvement in all aspects of this project has been truly appreciated. I would also like to thank my committee members, Dr. Michael Annable and Dr. Kirk Hatfield, for their guidance.

I would like to recognize my fellow EHL members, Dr. Huaguo Wang, Dr. Xiaosong Chen, Dr. Nandita Basu, Jango Bhadha, and Rajendra Paudel, for their daily friendship and collaboration. Special thanks go to Dan Perkins for his help with field equipment and to Dr. Jaeyhun Cho for his help with lab materials and methods. My most heartfelt appreciation is given to Julie Padowski for bequeathing me all of her PSFM knowledge, devoting herself to many hours field assistance, and being a wonderful friend. Lastly, I am especially grateful to Tom and my family for their endless love and encouragement.

TABLE OF CONTENTS

page

ACKNOWLEDGMENTS 4

LIST OF TABLES 7

LIST OF FIGURES 8

ABSTRACT 10

CHAPTER

1 INTRODUCTION 12

1.1 Background 12
1.1.1 Passive Sampling Devices 14
1.1.2 Methods for Determining Solute Load 16
1.1.3 Depth Sampling Apparatuses 19
1.2 Study Rationale 20
1.3 Previous Work 22
1.4 Hypotheses and Objectives 24

2 DEVICE THEORY AND CONSTRUCTION 26

2.1 Introduction 26
2.2 Passive Surface Water Flux Meter 26
2.2.1 Device Theory 27
2.2.1.1 Flow field determination 27
2.2.1.2 Steady-state flux determination 30
2.2.1.3 Transient flux determination 31
2.2.2 Device Design and Construction 33
2.2.2.1 Device body 33
2.2.2.2 Device cartridge 35
2.3 Constant Relative Depth Deployment Apparatus 38
2.3.1 Apparatus Theory 38
2.3.2 Apparatus Design and Construction 41

3 TRACER CHARACTERIZATION 45

3.1 Introduction 45
3.2 Laboratory Tracer Elution Tests 45
3.2.1 Elution Test Methods 46
3.2.2 Elution Test Results 48
3.3 Elution Test Modeling 53
3.3.1 Model Inputs and Methods 54
3.3.2 Model Results 58

3.3.3. Modeling Implications 61

4 STEADY-STATE FIELD DEPLOYMENT 66

4.1 Introduction 66
4.2 Deployment Site Description 66
4.3 Field Deployment Methods 71
4.4 Flux Measurements 73
4.4.1 Water Fluxes 74
4.4.2 Solute Mass Fluxes 76
4.5 Constant Relative Depth Deployment Apparatus Performance 79

5 TRANSIENT FIELD DEPLOYMENT 86

5.1 Introduction 86
5.2 Passive Surface Water Flux Meter Limitations 86
5.3 Transient Deployment Tests 88
5.3.1 Diurnal Deployment 91
5.3.2 Storm Deployment 93
5.4 Future Transient Testing and Development 94

6 CONCLUSIONS AND FUTURE WORK 96

LIST OF REFERENCES 99

BIOGRAPHICAL SKETCH 104

LIST OF TABLES

Table		page
3-1	Tracer mass balance during elution at various flow rates.	49
3-2	Retardation parameters derived from tracer elution profiles.	52
3-3	Inter-study comparison of tracer retardation factors.	52
3-4	Comparison of two methods for determining tracer retardation factors.	52
3-5	Solute transport parameters for elution test modeling.	55
3-6	Parameters for equilibrium and rate-limited tracer elution modeled in HYDRUS-1D.	59
4-1	Comparison of true and PSFM water fluxes during steady-state deployments.	75
4-2	Comparison of true and PSFM-derived steady-state phosphate mass fluxes.	77
5-1	Comparison of true and PSFM fluxes and loads during diurnal transient deployment.	93

LIST OF FIGURES

Figure		page
2-1	Design schematic for field-capable PSFM	27
2-2	Flow around an impermeable cylinder in the z_c-plane	28
2-3	Cylindrical PSFM device designed for field deployment	34
2-4	Sorptive media cartridge for field deployment	36
2-5	Laboratory apparatus for determining hydraulic conductivity (K_c)	37
2-6	Determination of cartridge hydraulic conductivity via Darcy's Law experiments	37
2-7	Design schematic for deployment of a cylindrical PSFM via CRD apparatus	40
2-8	Diagram depicting the intersection of a right triangle by a line parallel to its base	40
2-9	Diagram demonstrating maintenance of proportionality and constant relative depth as stream stage varies	41
2-10	Plan view schematic of the CRD deployment apparatus	42
2-11	Bead-bearings system to maintain orientation of PSFM cylinder	44
2-12	Equipment setup for field deployment of the cylindrical PSFM via CRD apparatus	44
3-1	Long-term tracer elution profiles	48
3-2	Linearization of the non-linear elution profiles of ethanol	51
3-3	Comparison of three predictions for tracer desorption	60
3-4	Experimental and modeled elution profiles for methanol, ethanol, IPA, and TBA	62
3-5	Ethanol elution curves fit with alternate equilibrium models	65
3-6	Extended simulations of IPA and TBA elution	65
4-1	Location and watershed delineation of PSFM field deployment site	67
4-2	PSFM deployment site in Sweetwater Branch	70
4-3	The PSFM and CRD apparatus deployed within Sweetwater Branch	71
4-4	Cross-sectional profiling of Sweetwater Branch water velocity	72

4-5 Data from SJRWMD monitoring station #01980199 74

4-6 Steady-state comparisons of true and PSFM water fluxes 76

4-7 Steady-state comparisons of true and PSFM phosphate *Jt* 78

4-8 CRD offsets required for various PSFM diameters and water depths 82

4-9 Error in the six-tenths relative depth positioning of the PSFM as water level fluctuates 84

4-10 Effect of streambed slope on CRD positioning of the PSFM 84

4-11 Errors in relative depth positioning of PSFM intake ports associated with sloping streambed. 85

5-1 Three scenarios for assessing PSFM versus time-series integration estimates of solute loading 89

5-2 Hypothetical TP fluxes generated from PSFM and time-series integration methods 90

5-3 Trends recorded in Sweetwater Branch during the diurnal deployment under normal flow conditions 92

5-4 Water depth in Sweetwater Branch before and during the storm event 95

Abstract of Thesis Presented to the Graduate School
of the University of Florida in Partial Fulfillment of the
Requirements for the Master of Science

FIELD-TESTING OF A PASSIVE SURFACE WATER FLUX METER FOR THE DIRECT MEASUREMENT OF WATER AND SOLUTE MASS FLUXES

By

Erin C. Atkinson

August 2007

Chair: James W. Jawitz
Major: Soil and Water Science

Measurement of water and solute mass discharges in surface water flow systems is a fundamental hydrologic task for ecological and economic decision making. However, because of the extensive monetary, labor, and time costs of traditional monitoring devices and methods, many water quality monitoring programs lack the resources necessary to provide comprehensive descriptions of surface water impairments. The Passive Surface Water Flux Meter (PSFM) is a recently developed passive sampling device that measures water and solute fluxes within flowing surface water bodies. Devoid of mechanical components and power supply requirements, the relatively low-maintenance, low-cost design of the PSFM gives it considerable potential as a tool for extensive, large-scale surface water quality characterization and monitoring. The novelty of the PSFM extends to its direct mass-based approach to solute flux measurement, as compared to conventional, indirect concentration-based approaches.

During this field-testing campaign, the PSFM was deployed at six-tenths relative depth in a flowing surface water body of north-central Florida. The device contained a dual-packed porous media cartridge that performed simultaneous ion exchange to determine phosphate mass flux and tracer desorption to determine average water flux within the stream. Development of the PSFM device used for this study included an in-depth characterization of tracer behavior within

the sorptive cartridge and the introduction of the constant relative depth (CRD) apparatus, a novel technology for maintaining monitoring equipment at constant relative depth despite variations stream stage.

The investigation of tracer behavior involved modeling laboratory elution of methanol, ethanol, IPA, and TBA within HYDRUS-1D. Results showed that while methanol and ethanol experience equilibrium desorption within the PSFM cartridge, IPA and TBA are better characterized by rate-limited non-equilibrium desorption. The degree of rate-limitation varies with both velocity and tracer retardation, and has implications for the use of IPA and TBA in flux determination over extended deployment durations.

The PSFM design described here was found to perform well in steady-flow conditions, demonstrating accurate measurement of steady-state water and phosphate mass fluxes to within 10%. The device was also shown to be effective under transient conditions of limited variability, but full transient field-testing remains for future work. Hypothetical scenarios demonstrated that the quadratic-mean nature of PSFM measurements may misrepresent true stream behavior under more pronounced transient conditions. While the CRD apparatus demonstrated is general applicability for constant relative depth sampling, it was determined not to be well suited for deployment of the PSFM design described here.

CHAPTER 1
INTRODUCTION

1.1 Background

Water quality degradation as a result of anthropogenic activities has been a growing concern within social and scientific communities for the past several decades. Specific surface water quality issues include increasing organic pollution, salinity, total suspended solids, heavy metals, nutrients, radionuclides, and acidification (Meybeck and Helmer, 1989). While extensive state and federal action has been taken to remediate easily identifiable point sources of pollution, less progress has been made with regard to nonpoint source pollution, such as excessive nutrient loads, because it is less tangible in the natural environment and therefore more difficult to address. Eutrophication caused by excessive inputs of phosphorus (P) and nitrogen (N) is currently one of the most common surface waters impairments in the United States, with agricultural and urban runoff as the leading sources of these nutrients to surface water bodies (Carpenter et al., 1998; Parry, 1998). The regulatory framework to deal with such nonpoint source pollution is already in place under the Clean Water Act, including parameters for the development and implementation of total maximum daily loads (TMDLs) for surface water contaminants of interest. However, monitoring programs remain deficient in terms of tools, resources, and ability to provide comprehensive descriptions of nonpoint source impairments and develop appropriate TMDLs (Cooter, 2004). This deficiency is especially detrimental when considering the ever-increasing regulatory recommendations for science-based TMDL development frameworks at both state and national levels, which require extensive monitoring and quantitative data collection (FDEP, 2006b; USEPA, 1999)

Traditional TMDL development can incur high costs due to the time, labor, and monetary expenses associated with monitoring equipment, data collection, and sample analysis. It is

already recognized that resource limitations have precluded the necessary application of in-depth assessment projects to impaired watersheds across the country, and it is unlikely that available funding for such endeavors will increases in the near future (Cooter, 2004). Further, TMDL development guidelines that encourage watershed monitoring approaches with minimal costs and promote the use of volunteer sampling programs also tend underrepresent water bodies that are small or of lesser public concern (USEPA, 1999). Hence, significant sources of contaminant loading may be easily overlooked due to restricted water quality characterization within a given watershed.

The Passive Surface Water Flux Meter (PSFM) is a recently developed passive sampling device, invented in an attempt to combat the resource limitations that are currently inhibiting the development of appropriate TMDLs. The PSFM utilizes resident tracers and sorptive porous media to directly measure cumulative water and solute mass fluxes within flowing surface water bodies through temporal integration of instantaneous water and solute mass fluxes (Klammler et al., 2007; Padowski, 2005). In the absence of mechanical components and power supply requirements, the relatively low-maintenance, low-cost design of the PSFM gives it considerable potential as a tool for extensive, watershed-wide surface water quality characterization and monitoring. The PSFM designs described by Padowski (2005) and Klammler et al. (2007) were applied for the measurement of phosphorus and nitrogen loads in laboratory settings, but could be easily adapted to measure other dissolved pollutants of interest by substituting appropriate sorbents. Hence, the PSFM has the capability to be a useful instrument for a variety of environmental applications including TMDL development, contaminant source identification, contaminant reduction evaluation, and aquatic ecosystem restoration evaluation. Further, the

PSFM displays true novelty in its innovative approach to passive, cumulative, mass-based water and solute measurement at constant relative depth.

1.1.1 Passive Sampling Devices

In its broadest sense, passive sampling can be defined as any sampling technique based on free flow of analyte molecules from the sampled medium to a receiving phase, as a result of a difference between the chemical potentials of the analyte in the two media (Vrana et al., 2005). Many passive samplers are able to provide cumulative (time-averaged) parameter estimates, offering an attractive alternative to traditional grab sampling methods. Instead of relying on the interpolation of discrete sampling and measurement, passive samplers can directly capture episodic events and allow for the concentration and detection of ultra-trace contaminants over time (Alvarez et al., 2005; Petty et al., 2004). Passive samplers also avoid the physical, logistical, and financial difficulties often associated with acquiring repetitive discrete samples, as well as the potential analytical bias associated with the storage and preservation of discrete surface water samples (Alvarez et al., 2005; Vrana et al., 2005; Worsfold et al., 2005; Burke et al., 2002; Jarvie et al., 2002).While mechanized methods for continuous real-time water quality monitoring are available, the associated equipment is generally expensive and particularly vulnerable to technology failure (Glasgow et al., 2004).This further highlights the low-cost, low-tech attractiveness of passive samplers.

A variety of passive sampling devices for the measurement of organic and inorganic pollutants in air, groundwater, and surface water have been developed since the 1970s, and many of these samplers are commercially available. The Interstate Technology & Regulatory Council (2006) classified cumulative aqueous samplers into two types: (1) devices that rely on diffusion of analytes to reach concentration equilibrium between the sampler and the water body and (2) devices that rely on diffusion to accumulate analytes within the sampler. The first device type

produces concentration samples that are time-weighted toward conditions during the latter portion of the deployment periods, due to the necessity of allowing two-way diffusion to establish equilibrium aqueous concentration at any given time. Examples of this device type include the nylon-screen passive diffusion sampler for measuring volatile organic compounds, the polyethylene diffusion bag sampler for measuring organic compounds and trace elements, and the rigid porous polyethylene sampler for measuring trace metals and perchlorate. The degree of time weighting experienced by these devices is typically dependent on analyte and device-specific diffusion rates (ITRC, 2006).

The second type of aqueous passive sampling device generates concentration samples that are time-averaged over the entire deployment period. Examples of this device type include the semi-permeable membrane device for measuring organic pollutants, the passive in-situ concentration extraction sampler for measuring volatile organic compounds, and the polar organic chemical integrative sampler for measuring pharmaceuticals, hormones, and herbicides. These devices incorporate semi-permeable membranes that allow the accumulation of solutes of interest, while excluding particulate matter, biogenic material, and potentially interfering substances(Alvarez et al., 2005).

There have also been recent developments in aqueous passive sampling devices that incorporate submerged bottles to collect time-averaged concentration samples, either via pressure-induced flow through a capillary hole or seepage through a permeable material (Selker and Rupp, 2005; Panno et al., 1998). In contrast to the aforementioned passive samplers, these devices allow for the collection of non-contaminant-specific samples, which can provide a more generalized description of water quality through analysis for a variety of solutes.

While these passive sampling devices each vary with regards to their underlying theory, design characteristics, and contaminants of interest, they all operate on concentration-based approaches to solute measurement. The samples they generate reflect either the concentration with which the device is at equilibrium or the time-averaged concentration to which it was exposed. Every passive sampler can be affected by environmental factors such as temperature, water turbulence, and biofouling so it is important to take these variables into account during device deployment and subsequent data analysis (Vrana et al., 2005). It is also essential to understand the temporal and spatial characteristics inherent to each device prior to deployment or data comparison, because under certain conditions they may provide different, but equally valid representations of a given hydrologic setting (ITRC, 2006).

1.1.2 Methods for Determining Solute Load

Estimation of solute load, defined as the solute mass transported across a boundary during a specified time period, is frequently the central objective in research studies and water quality monitoring programs, such as TMDL development (Aulenbach and Hoopert, 2006). Determination of solute loads within flowing surface water bodies requires measurement of both stream discharge and solute concentration, and is given by

$$M_Q = \int C(t)Q(t)dt \qquad (1\text{-}1)$$

where M_Q [MT^{-1}] is solute load, C [ML^{-3}] is solute concentration, Q [L^3T^{-1}] is stream discharge, and t [T] is time.

There are numerous standardized methods for measuring stream discharge (flow), both directly and indirectly (BOR, 2001; Herschey, 1985). Direct methods include tracer dilution experiments, ultrasonic measurement devices, and electromagnetic measurement devices. The dilution method involves injecting liquid tracer into a flowing steam. Discharge is derived from

the change in concentration between the injected solution and downstream water samples. Ultrasonic devices transmit simultaneous ultrasonic pulses in two directions across a flowing stream channel, and the difference in the pulse transit time is used to derive discharge. Electromagnetic devices measure the electromotive force produced by flowing water, which is proportional to discharge (BOR, 2001; Herschey, 1985).

Indirect methods are those that use measurements of either water head or velocity to determine stream discharge. Devices that measure head and determine discharge based on known pressure relationships and equations include weirs, flumes, and orifices. Velocity measurements are utilized in stream gauging methods, which derive discharge from the sum of the products of stream velocity, depth, and distance between vertical measurements (Herschey, 1985). The velocity measurements are generally made with a current meter (anemometer, acoustic Doppler, or optical strobe) according to a certain cross-sectional transect protocol, such as the six-tenths, two-point, or depth integration method (BOR, 2001). Stream gauging over a range of hydrologic conditions can generate a steam-specific stage-discharge relationship. Once established, this relation can be used to derive discharge from measurements of stream stage alone (Herschey, 1985).

Selection of the most appropriate method for discharge determination in a given surface water body is dependent on several hydrologic, economic, and logistical factors. Hydrologic factors that should be considered for all methods include velocity distribution and range, geometry of the channel, turbulence, and backwater conditions. Available head loss, bed conditions, and channel width should also be assessed when considering the installation of weirs or flumes. Economic factors include the capital available for the cost of equipment, installation, maintenance, staffing, and data processing. While some methods, such as stream gauging and

weirs/flumes, are relatively inexpensive to maintain after initial investment, other methods, such as tracer dilution, include additional costs whenever they are employed. Logistical factors to consider include site accessibility, maintenance frequency, and availability of electrical power (Herschey, 1985).

Measurements of solute concentration can be obtained from several water sampling techniques. These techniques include manual grab sampling, automated discrete sampling devices (i.e., autosamplers), and passive sampling devices. Manual grab sampling involves minimal equipment, but may be impractical for routine or large-scale sampling due to transportation and time requirements. Autosamplers can reduce labor costs and provide more frequent sampling, but their use introduces concerns with sample preservation and contamination (Clesceri et al., 1998). Passive sampling devices, such as the aforementioned diffusion-type and submerged bottle samplers, can reduce preservation and contamination concerns and provide time-averaged samples for the estimation of solute concentration.

Once discharge and concentration measurements have been acquired, solute load can be estimated through mathematical manipulation of the data. Given the instantaneous nature of water discharge measurements, the cumulative discharge required for solute load calculation must be obtained from interpolating and integrating the time series data (Klammler et al., 2007). Further, unless a passive sampling device is used, solute concentration data must also be interpolated and integrated over the time period of interest. There are several published approaches that can be used to perform the necessary time averaging of discharge and concentration data and estimate solute load. These include averaging methods, period-weighted approaches, regression-model (or rating-curve) methods, ratio estimators, and composite methods. The appropriate method to use depends on the frequency and distribution of sampling

and the strength and form of the relationship between other variables, such as discharge and season (Aulenbach and Hoopert, 2006). However, no matter which approach is employed, solute mass load is always indirectly calculated from concentration data.

1.1.3 Depth Sampling Apparatuses

Standard methods indicate that the velocity measured at a relative depth of 0.6 below the water surface represents average stream velocity (BOR, 2001). However, while there is little documentation of equipment for deploying monitoring devices at specified relative depths, bottom-mounted and moored apparatuses for the deployment of instruments at target depths are abundant within the hydrologic and oceanographic literature. Such apparatuses can act as individual monitoring stations when installed singularly, or strategies can include several simultaneous deployments to create larger-scale monitoring arrays. Instruments and sensors to measure a variety of water quality parameters, such as temperature, salinity, pressure, conductivity, velocity, turbidity, fluorescence, chlorophyll, and dissolved oxygen, as well as a variety of sampling devices can be attached and deployed with depth sampling apparatuses (Branco et al., 2005; McManus et al., 2003).

In general, apparatuses are constructed to maintain instruments at either a fixed absolute depth or over a fixed depth profile. Apparatuses designed to maintain measurement at fixed absolute depths are either bottom-mounted to hold an instrument at a specified depth, or can employ moored buoys to suspend instruments from the water surface. Water level fluctuations must be taken into account when deploying a bottom-mounted apparatus, as significant decreases in water depth have the potential to expose instrumentation. Alternatively, moored buoys allows the desired absolute depth of the instrument to remain constant as water level varies (Chuang, 2002; Panno et al., 1998).

Depth profiling apparatuses can also be bottom-mounted or moored, and are generally employed in aquatic and marine systems with minimal water level fluctuations. Profilers usually incorporate either a winch system or variable buoyancy sensors coupled with dynamic buoyancy compensators to convey instruments along a vertical profile of target depths (Branco et al., 2005; Tokhtuev et al., 2005; Ward et al., 2004; McManus et al., 2003). Systems can be designed to automatically profile to fixed depths at specified times, or can be remotely controlled to transport instruments to given depths whenever monitoring is desired. Both approaches require the depth profiler apparatus to contain expensive mechanized parts that are often susceptible to corrosion and biofouling (Branco et al., 2005).

1.2 Study Rationale

The PSFM meets the broad definition of a passive sampler outlined by Vrana et al. (2005) through its use of sorptive resin to retain a representative portion of solute from the sampled water body. However, the PSFM measures solute mass fluxes from a novel mass-based approach, rather than the concentration-based approaches employed when using either active sampling approaches (e.g., autosamplers), or other passive sampling devices. The PSFM provides concurrent, direct measurements of cumulative water flux (velocity) and cumulative solute mass flux (Klammler et al., 2007). Direct measurement of solute mass for determination of solute flux is preferred to concentration-based approaches where mass is indirectly obtained from solute concentration. The concurrent measurements of water and solute mass fluxes also make it possible to generate flux estimates that reflect long-term transport conditions, incorporating fluctuations in both water flow and solute load (Hatfield et al., 2004).

Through its dual measurement of water and solute mass fluxes, the PSFM generates a more comprehensive water body characterization than traditional passive samplers, moving beyond purely solute measurement to the evaluation of additional descriptive parameters. In addition to

the chemical characterization performed by all passive samplers, the measurement of cumulative water velocity allows for simultaneous physical characterization of a surface water body, thus extending applicability of the PSFM. This is especially relevant considering the relative simplicity of the PSFM when compared to current methods of solute load measurement, which generally involve extensive time and labor costs and require a variety of expensive equipment for measurement and sampling (weirs, flumes, velocity meters, autosamplers, etc.). The PSFM also provides continuous time-averaged flux measurements, eliminating the need for complex mathematical methods of interpolation and integration to estimate solute loads. Further, flux could be considered a more useful quantity for characterizing solute transport in streams, because in contrast to solute load calculation, its description of solute mass transport on a per area basis does not require knowledge of channel cross-sectional area, which is often difficult to determine with accuracy in natural systems (Padowski, 2005). However, despite the many positive aspects of PSFM use for surface water monitoring, there are also some limitations to its performance, specifically that the device provides only end-point data with no insight into how fluxes varied over a given deployment duration.

When combined with a constant relative depth (CRD) deployment apparatus, the measurements taken by the PSFM become standardized and its utility further increases. The CRD apparatus introduced here has been designed to allow for continuous sampling and measurement at six-tenths relative depth, the location of average stream velocity, regardless of varying stream stage. The CRD apparatus may also be applied for other relative depth methods (e.g. 0.2 and 0.8 depths method), and has extended application for the deployment of a variety of surface water monitoring instruments, including an assortment of probes, sensors, meters, passive samplers, and autosamplers. For instance, pairing the CRD apparatus with a velocity

meter has potential as an alternative to tracer studies and stream gauging for determining average stream velocity (Waldon, 2004). The CRD apparatus is different from traditional depth sampling apparatuses in that it provides passive, automatic, and continuous deployment at a given relative depth, rather than confining instruments to fixed absolute depths that may miss average stream behavior during significant water level changes or requiring manual mechanization to maintain the relative depth position over the deployment duration.

Using the CRD apparatus for PSFM deployment ensures that water and solute flux measurements are constantly reflective of the average velocity conditions in a flowing surface water body, regardless of water level fluctuations. The passive, low-cost nature of the CRD apparatus couples particularly well with the PSFM, because neither device has mechanical parts or power supply requirements. The CRD apparatus also ensures that the PSFM is constantly submerged over its entire deployment duration, eliminating concerns regarding PSFM port exposure and column desaturation due to variations in stream stage (Klammler et al., 2007).

1.3 Previous Work

The conceptual model for the PSFM was developed as a partner device to the Passive Flux Meter (PFM), which measures contaminant and groundwater fluxes in saturated porous media (Annable et al., 2005; Hatfield et al., 2004; Hatfield et al., 2002). Similar to the PSFM, the PFM utilizes sorptive media and resident tracers to estimate water and solute fluxes.

Hatfield et al. (2004) validated the PFM theory through a series of laboratory box-aquifer experiments. Water flux measurements made with the PFM were found to be most accurate when tracers were eluted to 20-70% of initial conditions, and PFM-estimated solute fluxes were found to be within 5% of the true solute flux. The study also characterized the linearization of non-linear tracer elution processes, which is necessary for proper determination of the tracer retardation factors (R_d).

Annable et al. (2005) demonstrated the successful field deployment of the PFM and verified its use as a tool for assessing and monitoring groundwater contamination in screened wells at hazardous waste sites. The PFM-measured groundwater fluxes were within 15% of imposed (controlled) fluxes, and solute fluxes were measured within 30% of fluxes measured via well extraction.

Klammler et al. (2004) first presented the PSFM theory and conceptual model. Subsequently, Padowski (2005) designed several sorptive-media columns and tested cylindrical and hydrofoil PSFM devices to validate the conceptual model within a laboratory setting. A cartridge design containing sorptive resin and tracer-impregnated granular activated carbon packed in series was chosen for use in the PSFM, and the hydraulic conductivity and non-linear tracer elution processes (specifically retardation factor) of the column media were determined through laboratory experiments. The cylindrical and hydrofoil PSFMs were both tested in a series of flume experiments over a range of controlled stream flows and solute (phosphate) concentrations. Water and phosphate fluxes calculated from independent measurements of velocity (acoustic Doppler velocimeter) and head difference across the column (manometers) were compared to resin-sorption and tracer-elution-derived fluxes to determine the accuracy of the PSFM. Results showed that PSFM-derived water fluxes differed from true water flux by approximately 25%, and PSFM-derived phosphate fluxes differed from true solute flux by approximately 30%. It was also found that the cylindrical PSFM performed well over the entire range of velocities tested, while the hydrofoil-shaped PSFM performed poorly at lower velocities due to its inability generate enough head difference across the cartridge to maintain steady flow.

Klammler et al. (2007) conducted laboratory flume experiments to investigate the hydraulic performance of a hydrofoil PSFM, as well as the hydraulic and sorptive properties of

its sorbent cartridges. The cartridge design included two separate columns in series; the first packed with anion exchange resin for the sorption of nitrate, and the second packed with tracer-impregnated activated carbon. Instantaneous water fluxes obtained from independent Pitot-tube flow velocities were compared to instantaneous water fluxes derived from the head differences across several combinations of PSFM ports. Results showed these measurements to have a mean error of approximately 5% over water velocities ranging from 30 to 70 cm/s. Cumulative water and solute mass fluxes were also compared between PSFM-estimated values obtained from remaining tracer and absorbed nitrate masses in the sorbent cartridge and values obtained from Pitot-tube measurements and nitrate concentration grab sampling of flume water. Results showed good agreement for cumulative water fluxes over a range of 50 to 600 L/cm^2 ($R^2 = 0.99$) and for cumulative nitrate fluxes ranging over a range of 0.4 to 5.1 g/cm^2 ($R^2 = 0.98$). A sensitivity analysis was conducted to investigate the sources and propagation of error within the PSFM flux calculations, and it was determined that in order to avoid the generation of large absolute errors in flow velocity, PSFM ports should be positioned such that the local flow velocities at their locations are sufficiently different. The study also introduced a correction factor to the flux calculations that accounts for the restriction of the flow domain to a channel of specified width.

Despite its relatively simple design and great potential for utility, no previous work involving a constant-relative-depth-type deployment apparatus could be found within the scientific literature. Hence, the CRD apparatus introduced in this study is considered to be a truly novel approach for the deployment of surface water measurement and sampling instruments. The preliminary procedures for patenting this technology are currently underway.

1.4 Hypotheses and Objectives

Given the previous laboratory research conducted on the PSFM and potential utility of the CRD apparatus, field-testing was a logical next step within the development of both devices.

Successfully transitioning the PSFM from the controlled conditions of the lab to the complex variability of natural streams required a more precise understanding of resident tracer behavior within the sorptive cartridge and an assessment of its field performance over a variety of environmental conditions (both steady-state and transient). As such, this study aimed to investigate three hypotheses:

- In accordance with the assumptions of PSFM theory, resident tracers experience mass balance and equilibrium desorption within the sorptive media cartridge.
- Similar to its performance in laboratory settings, the PSFM accurately measures water and solute mass fluxes in natural stream channels.
- Using a floating arm and the geometry of similar triangles, the CRD apparatus allows for accurate measurement of stream conditions at the depth of average velocity, regardless of fluctuations in stream stage.

The following set of objectives were used to test these hypotheses:

- Characterize tracer behavior within the PSFM sorptive cartridge through laboratory elution tests and HYDRUS-1D modeling.
- Design and construct a field-ready PSFM with CRD deployment apparatus.
- Deploy the PSFM via CRD apparatus for experimental data collection in natural stream channels.
- Investigate and verify the ability of the PSFM to accurately measure water and solute mass fluxes under both steady state and transient surface water conditions.
- Evaluate the ability of the CRD deployment apparatus to sustain water-monitoring instrumentation at a specified relative depth under natural stream conditions.

CHAPTER 2
DEVICE THEORY AND CONSTRUCTION

2.1 Introduction

The Passive Surface Water Flux Meter represents a novel approach for the direct measurement of cumulative water and solute mass fluxes in flowing surface water bodies. Its low-cost, low-maintenance design makes it an appealing alternative to traditional, interpolative methods of solute flux determination in streams. Deploying the PSFM at six-tenths (of total depth) below the water surface ensures that the device will capture measurements representative of the depth-averaged velocity at a given lateral location within the stream.

However, in surface flow systems that experience water level fluctuations, the location of six-tenths relative depth is not fixed. As stream stage and total depth vary, so does the absolute location of a given relative depth. Hence, a deployment strategy, such as the CRD apparatus, that can constantly maintain instrumentation at a given relative depth provides an attractive method for capturing conditions within the average velocity regime.

2.2 Passive Surface Water Flux Meter

The PSFM consists of a permeable cartridge attached to an external body that is inserted into flowing surface water, normal to the flow direction. The cartridge is packed with sorptive resin and tracer-impregnated granular activated carbon in series, and is connected to small openings (ports) on the external surface of the body (Figure 2-1). During deployment, velocity and pressure distributions resulting from the flow field around the external body induce water flow through the cartridge. After deployment, the resin-sorbed solute and remaining tracers are extracted and the masses obtained are proportional to water and solute flux in the external flow field.

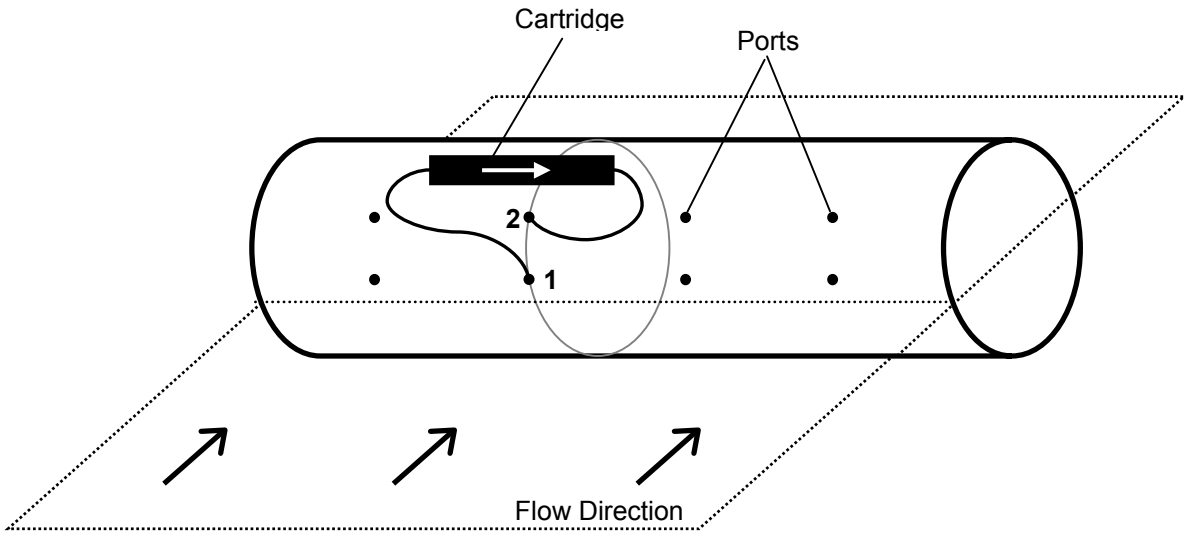

Figure 2-1. Design schematic for field-capable PSFM. The cylinder is inserted within the flow field normal to flow direction. Water flows through the cartridge, entering via port 1 and exiting through port 2.

2.2.1 Device Theory

Klammler et al. (2007) outlined the mathematical theory and conceptual model for estimating water and solute mass fluxes by determining the velocity and pressure distributions around a submerged PSFM. There are several conditions that must be met during PSFM deployment to stabilize the pressure distribution around the body and allow for accurate water and solute flux calculations: disturbances to the flow field should be minimal when the PSFM is inserted within flowing surface water, and both the generation of wakes and device vibrations should be avoided.

2.2.1.1 Flow field determination

The solution for uniform potential flow around an impermeable, circular cylinder (Figure 2-2) can be determined via conformal mapping and is known to be (Milne-Thomson, 1960)

$$\Omega(z_c) = v_o \cdot \left(z_c + \frac{a^2}{z_c} \right) \tag{2-1}$$

where $\Omega = \Phi + i\Psi$ is the complex potential with Φ representing the potential function and Ψ

representing the stream function, $z_c = x_c + iy_c$ are complex coordinates of a point in the cross-sectional plane of the cylinder containing the impermeable circle with radius a [L], and v_o [L/T] is the velocity of the flow field at $x = -\infty$.

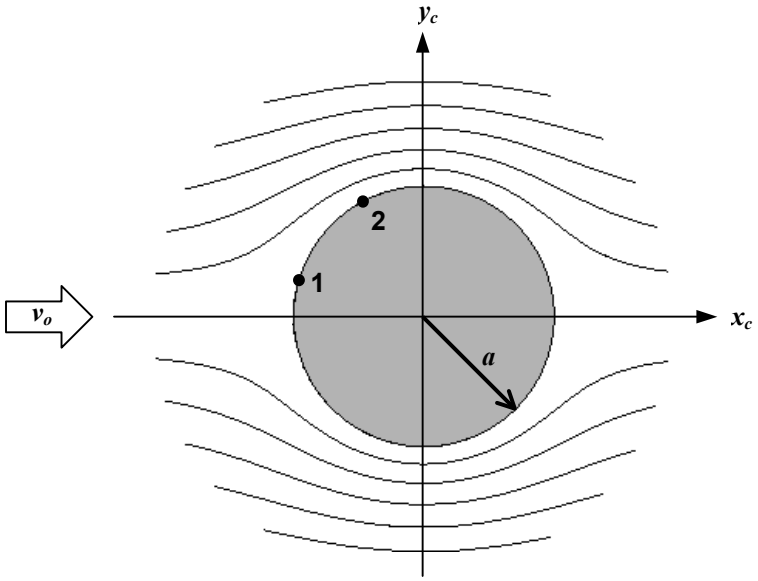

Figure 2-2. Flow around an impermeable cylinder in the z_c-plane. Port 1 is exposed to lower water velocity and higher pressure, while port 2 is exposed to higher water velocity and lower pressure. This results in a pressure gradient that induces water flow from port 1 to port 2.

The PSFM theory based on this flow field was detailed by Klammler et al. (2007) and its use for both steady-state and transient flux determination are summarized here. The complex potential of the flow field can be related to the complex coordinates at any point on the PSFM by

$$z_j = \left[z_c - (1-b)\cdot a\right] + \frac{(a\cdot b)^2}{\left[z_c - (1-b)\cdot a\right]} \tag{2-2}$$

where $z_j = x_j + iy_j$ are the transformed complex coordinates of the PSFM profile in the z_j-plane, and b [-] is a parameter defining the shape of the resulting profile. The value of b ranges from zero for a cylindrical, blunt profile to one for a straight, slender profile.

Using the complex coordinates, the distribution of flow velocity around the body can be determined by Equation 2-3,

$$v_j = \frac{v_o \cdot \left|1 - \frac{a^2}{z_c^{\,2}}\right|}{\left|1 - \frac{(a \cdot b)^2}{[z_c - (1 - b \cdot a)]^2}\right|} = v_o \cdot \chi_i \tag{2-3}$$

where v_j [L/T] is the complex conjugate of the flow velocity around the body at a given point, v_o [L/T] is the velocity of the flow field at that point, and χ_i [-] are proportionality constants dependent on the shape of the PSFM and the location of the port openings.

Once flow velocity is known, the static pressures at these points can be determined from Bernoulli's equation

$$\Delta H = \left[\frac{p_1}{\rho g} + \frac{v_1^{\,2}}{2g} = \frac{p_2}{\rho g} + \frac{v_2^{\,2}}{2g}\right] = \left[\frac{1}{\rho g} \cdot (p_1 - p_2) = \frac{1}{2g} \cdot \left(v_1^{\,2} - v_2^{\,2}\right)\right] \tag{2-4}$$

where ΔH [L] is the static pressure head difference, p_1 and p_2 [M/LT^2] are the static pressures at ports 1 and 2, respectively, v_1 and v_2 are the flow velocities at ports 1 and 2, respectively, ρ [M/L^3] is the density of water, and g [L/T^2] is gravitational acceleration. From Equation 2-3, both v_1 and v_2 can be expressed as proportional to v_o, which is the actual variable of interest,

$$\begin{aligned} v_1 &= \chi_1 v_o \\ v_2 &= \chi_2 v_o \end{aligned} \tag{2-5}$$

Equation 2-3 allows for calculating χ_1 and χ_2. However, to account for the fact that the flow domain is not infinite but restricted to a specified channel width, each χ_i proportionality constant must be multiplied by a correction factor before use in subsequent calculations. These correction factors, α_i [-], invoke the law of continuity and are given by

$$\alpha_i = \frac{w_c}{(w_c - w_p)} \tag{2-6}$$

where w_c [L] is the channel width and w_p [L] is the width of the PSFM profile at a given port location.

Equations 2-3 and 2-4 can then be combined to yield water flux (velocity), v_o [L/T]

$$v_o = \sqrt{\frac{2g}{(\alpha_2\chi_2)^2 - (\alpha_1\chi_1)^2} \cdot \left(\frac{p1}{\rho g} - \frac{p2}{\rho g}\right)} = \sqrt{\left(\frac{2g}{(\alpha_2\chi_2)^2 - (\alpha_1\chi_1)^2}\right) \cdot \Delta H} \qquad (2\text{-}7)$$

where ΔH represents the head difference between ports 1 and 2. Heads at ports 1 and 2 have been measured directly in laboratory validation experiments (Klammler et al., 2007; Padowski, 2005), but during field deployment these must be determined from the relative amount of tracer remaining on the cartridge using

$$\Delta H = \left(\frac{p_1}{\rho g} \cdot \frac{p_2}{\rho g}\right) = \left(1 - M_{t,r}\right) \cdot \frac{L_c L_t \theta R_d}{K_c t_d} \qquad (2\text{-}8)$$

where $M_{t,r}$ [-] is the relative mass of the tracer remaining after elution with respect to the initial tracer mass, L_c [L] is the length of the entire cartridge, L_t [L] is the length of the tracer-impregnated portion of the cartridge, θ [-] is the water content of the porous media, R_d [-] is the retardation factor of the tracer, and K_c [LT^{-1}] is the hydraulic conductivity of the porous media within the cartridge, and t_d [T] is the deployment duration. The retardation factor, R_d, is derived from laboratory experiments and the linearization of non-linear elution curves (Hatfield et al., 2004).

2.2.1.2 Steady-state flux determination

For PSFM deployment durations short enough that it is reasonable to assume that field conditions of water velocity and solute concentration will be constant over time, stream water and solute mass fluxes may be calculated via a series of steady-state equations. Assuming steady-state water velocity, flow through the cartridge, Q_c [L^3/T], results from Darcy's Law as

$$Q_c = \frac{K_c A \Delta H}{L_c} \tag{2-9}$$

where A [L^2] is the cross-sectional area of the cartridge. Equations 2-8 and 2-9 can be combined and Q_c can be calculated by

$$Q_c = \frac{\left(M_{t,r} - 1\right) A \theta R_d L_t}{t_d} \tag{2-10}$$

Then, average solute concentration in the stream flow, C_s [M/L^3], can be determined by

$$C_s = \frac{M_s}{Q_c \cdot t_d} \tag{2-11}$$

where M_s [M] is the solute mass retained by the sorptive resin. Solute mass flux, J_s [$ML^{-2}T^{-1}$] can subsequently be calculated as

$$J_s = v_o C_s = \frac{2 g L_c M_s}{t_d v_0 A K_c \left(\left(\alpha_2 \chi_2\right)^2 - \left(\alpha_1 \chi_1\right)^2\right)} \tag{2-12}$$

where Equations 2-7, 2-9, and 2-16 have been substituted to eliminate C_s, Q_c, and ΔH. It is important to note that the estimates of v_o, C_s, and J_s calculated by this method are obtained as time averages over the duration of deployment.

2.2.1.3 Transient flux determination

Flowing surface water systems often exhibit variations in water velocity, depth, and solute concentration over extended time periods due to natural cycles or storm events. As such transient conditions are likely to be encountered during longer-duration PSFM field deployments, it is important to have a quantitative framework for analyzing these data. However, analysis of transient PSFM data can be somewhat complicated given the mathematical limitations of the theory and conceptual model.

Klammler et al. (2007) show that as water velocity and solute concentration vary with time, theoretically derived estimates of these parameters lose some of their physical meaning. Under transient conditions, the PSFM actually measures the quadratic mean of the flow velocity, rather than the desired arithmetic mean. The difference between these means can be significant if there is considerable variation in flow velocity over the deployment duration. Further, estimates of solute concentration have to be regarded as the flux averaged solute concentration in the sorptive cartridge, which is no longer equivalent to the flux averaged solute concentration in the stream. Yet in spite of these complexities, there are several assumptions that can be made to return significance to PSFM measurements made under transient conditions and allow for meaningful, albeit limited, interpretation of such results.

If it is assumed that the variation in flow velocity of a given system is sufficiently small, then the arithmetic mean, $v_{0,ar}$ [L/T], can be approximated well by the measured quadratic mean, $v_{0,sq}$ [L/T], as given by

$$v_{0,sq} = \sqrt{\frac{v_{0,ar}^2}{t_d}\int_0^{t_d} dt} \approx v_{0,ar} \tag{2-13}$$

Additionally, if it is assumed that either variation in solute concentration is small over time or that variations in solute concentration and water velocity are uncorrelated, then the arithmetic average of the actual solute flux, $J_{s,ar}$ [M/L^{2}T], can be given by

$$J_{s,ar} \propto \frac{M_s}{t_d v_{0,ar}} \tag{2-14}$$

This indicates, under the conditions stated above, that the solute mass flux estimated from Equation 2-12 can be regarded as $J_{s,ar}$. It is recalled that v_0 in Equation 2-12 was assumed constant and, hence, is equivalent to the respective $v_{0,ar}$ in Equation 2-14.

Similar to the steady-state equations, the estimates of $v_{0,ar}$ and $J_{s,ar}$ calculated by this method are still obtained as time averages over the duration of deployment. This implies that no estimates of the timing or range of water velocity and solute concentration fluctuations can be made directly from transient PSFM measurements made via the sorptive cartridge. Further, if the variations in flow velocity and solute concentration are not small or the variations are correlated, flux estimates derived from these calculations are likely to be inaccurate.

2.2.2 Device Design and Construction

Design and construction of the cylindrical PSFM device for this study was similar to that outlined by Padowski (2005) for flume deployment. However, several modifications were made to prepare and customize the PSFM for successful field deployment via the CRD apparatus. The most significant modification was the horizontal, rather than vertical, positioning of the cylinder within the flow field, which provides multiple flux measurements at a given depth, rather than a depth profile of flux measurements.

A cylindrical body design was chosen for this study instead of a hydrofoil because flume experiments demonstrated that the cylinder was able to generate sufficient head difference to maintain steady flow within the sorptive cartridge over a wider range of stream velocities (Padowski, 2005). Superior performance at lower velocities made the cylinder an obvious choice for initial field-testing, where unpredictable and fluctuating stream velocities could be encountered. Phosphate (PO_4^{3-}) was the solute of interest measured by the field-ready PSFM, because phosphorus tends to be the most limiting nutrient in freshwater bodies (Parry, 1998).

2.2.2.1 Device body

The cylindrical body of the PSFM was constructed from 98 cm of rigid PVC pipe, with an inner diameter of 10 cm and an outer diameter of 11.4 cm (Figure 2-3). The port pairs for intake and outlet from the sorptive cartridge were positioned laterally along the cylinder, approximately

every 10 cm. Each port measured 0.3 cm in diameter. With the cylinder aligned normal to the flow direction such that water flowed from 180º to 0º (Figure 2-2), the intake ports were located 7.5 cm along the cylinder circumference (77º), where the vertical profile width was 3.2 cm. The outlet ports were located at 2 cm along the cylinder circumference (20º), where the vertical profile width was 10.2 cm. These port locations were chosen based on flume results showing this positioning to produce the greatest head difference across the sorptive cartridge, resulting in the most stable flow through the cartridge (Padowski, 2005). Chi-values (χ_i) were calculated from Equation 2-3 as $\chi_1 = 1.99$ for the intake ports and $\chi_2 = 0.96$ for the outlet ports. As stream width varied between individual field deployments, corrected chi-values were recalculated for the most accurate water and solute mass flux determination.

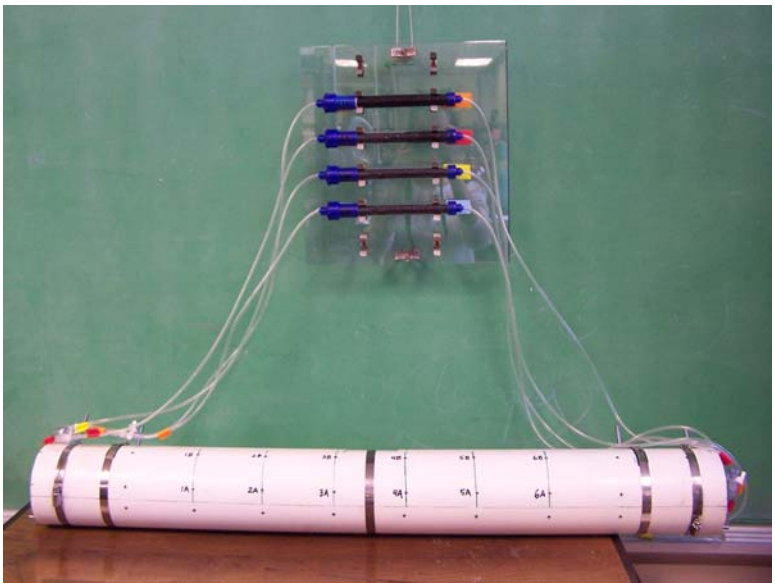

Figure 2-3. Cylindrical PSFM device designed for field deployment, including exterior cartridge mount.

The sorptive cartridges were mounted to an exterior rack for easy cartridge exchange during field deployment and were attached to the intake and outlet ports via lengths of Tygon tubing. Three-way Luer-lock valves were installed midway between cylinder and cartridges for

water priming, purging, and dye injection to confirm flow through the cartridges. The bottom of the cylinder (270º in Figure 2-2) was lined with weights to ensure maintenance of the proper port orientation within the stream. These weights were attached to the interior of the cylinder, so as not to disrupt the flow field around the device.

2.2.2.2 Device cartridge

The sorptive media cartridges used with the cylindrical PSFM body were constructed using Kontes borosilicate glass columns of 19 cm length and 1.5 cm diameter, fitted with 500 μm polypropylene mesh filters to prevent the loss of sorptive media during flow. The first 4 cm of each cartridge were packed with anion exchange resin (Lewatit S6328A) for the sorption of phosphate, and the remaining 15 cm were packed with silver-impregnated granular activated carbon (Barneby Sutcliffe 989_12_30) that was pre-equilibrated with a suite of resident tracers (Figure 2-4). Effectiveness of these sorptive media for flux calculation was determined by Annable et al. (2005) and Padowski (2005). Tracer pre-equilibration involved rotating the activated carbon with an aqueous solution containing 1200 mg/L methanol, 1200 mg/L ethanol, 2300 mg/L isopropyl alcohol, 2300 mg/L tert-butyl alcohol, and 1200 mg/L 2,4-dimethyl-3-pentanol for 24 hours (Annable et al., 2005). Both the resin and activated carbon were wet-packed as a slurry with deionized water to ensure cartridge saturation, and a handheld vibrator was used to guarantee tightest particle packing and to release any trapped air. To prevent mixing between the resin and activated carbon that would complicate the post-deployment extraction procedures, a thin layer of glass wool was inserted to separate the two media types.

Determination of cartridge water content (θ) and hydraulic conductivity (K_c) was required for subsequent modeling of tracer elution and calculation of water and solute mass fluxes during field deployment. Wet-dry gravimetric analysis of the activated carbon established the water

content of the activated carbon to be 0.6. This value compares reasonably well with the water content of 0.55 determined by Annable et al. (2005) for the same material. The analysis also determined the pore volume and bulk density of the activated carbon portion of the cartridge to be 15.95 mL and 0.66 g/cm^3, respectively.

Figure 2-4. Sorptive media cartridge for field deployment, packed in series with anion exchange resin (4cm) and tracer-impregnated activated carbon (15 cm).

Hydraulic conductivity of the cartridge was determined via Darcy's Law experiments. The cartridge was connected to a constant head reservoir (10-L Mariotte bottle) of deionized water, and the height of the reservoir was periodically adjusted to create a series of manometer-measured pressure head gradients (ΔH) across the cartridge (Figure 2-5). For each specific head gradient, discharged water was collected and measured to determine flow through the cartridge (Q_c). Darcy's Law was then used to calculate K_c by

$$q = \frac{Q_c}{A} = -K_c \frac{\Delta H}{\Delta L} \tag{2-15}$$

where q [LT^{-1}] is specific discharge and $\Delta H/\Delta L$ [-] is the hydraulic gradient.

Two sets Darcy's Law experiments and calculations were conducted to generate K_c values for two separate components of this study. The first experiment replicated the conditions of the laboratory investigations of tracer elution, and generated a hydraulic conductivity of K_c=28.8 cm/min (Figure 2-6A). The second experiment replicated the conditions of PSFM field

deployments, and generated a hydraulic conductivity of K_c=23.0 cm/min (Figure 2-6B). The main difference between the two experimental setups was the length of tubing connected to either end of the sorptive cartridge. The field deployment setup required longer lengths of tubing, which created greater head loss within the system, resulting in decreased hydraulic conductivity as compared to the elution test setup.

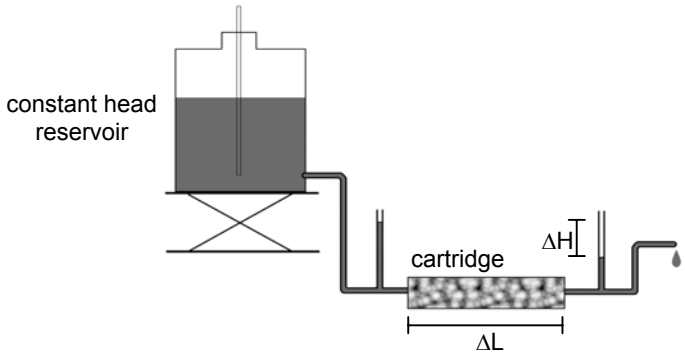

Figure 2-5. Laboratory apparatus for determining hydraulic conductivity (K_c) of the sorptive cartridge via Darcy's Law. The hydraulic gradient created by adjusting the height of the constant head reservoir is directly proportional to flow through the cartridge. (Adapted from Padowski, 2005)

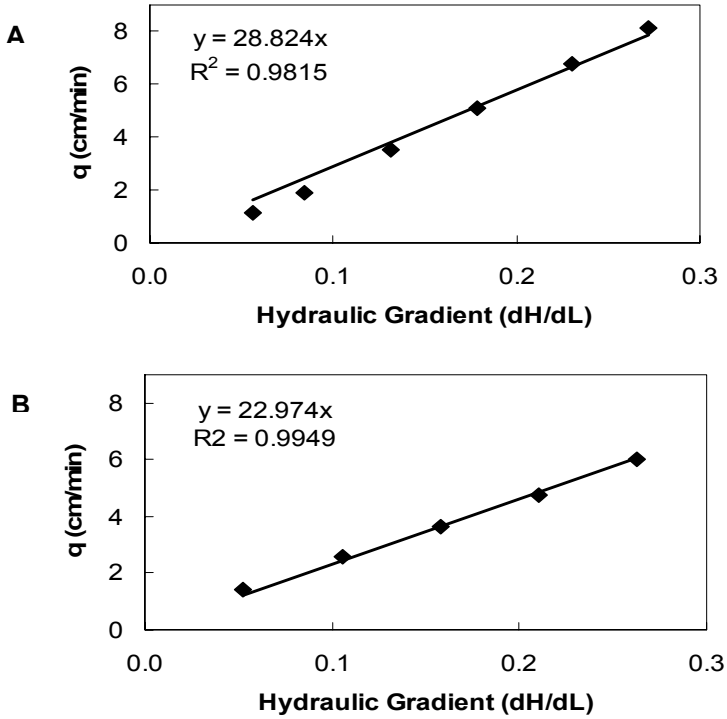

Figure 2-6. Determination of cartridge hydraulic conductivity via Darcy's Law experiments. A) For the tracer elution test setup. B) For the field deployment setup.

2.3 Constant Relative Depth Deployment Apparatus

2.3.1 Apparatus Theory

Observed velocity profiles within natural channels generally indicate turbulent, rather than laminar, flow (Hornberger et al., 1998). The vertical velocity distribution of turbulent channel flow, *u(z)* [L/T], is given by the Karman-Prandtl equation

$$u(z) = \sqrt{gR_H S}\left[2.5\ln\left(\frac{z}{k_r}\right) + 8.5\right] \tag{2-16}$$

where R_h [-] is the hydraulic radius defined as the ratio of the channel cross-sectional area to the wetted perimeter, S [-] is channel slope, k_r [-] is a channel roughness parameter, and z [L] is vertical location within the water column, with $z = 0$ defined as the bottom of the water column (Hornberger et al., 1998; Montes, 1998).

Mean velocity in a channel, U [L/T], is the integral of the velocities as each point in a cross section divided by the cross-sectional area, A [L^2]

$$U = \frac{1}{A}\int_0^w \int_0^h u(y,z)\, dz\, dy \tag{2-17}$$

where w [L] is width of the channel, h [L] is depth of water, and y [L] is lateral location within the stream. Given that the Karman-Prandtl equation describes only how velocity varies in the vertical direction (z), it is here assumed that the channel is wide and rectangular and that velocity does not vary laterally across the channel. Thus, integrating across the channel is equivalent to multiplying by channel width, and Equation 2-17 simplifies to

$$U = \frac{1}{wh} w\int_0^h u(z)\, dz = \frac{1}{h}\int_0^h u(z)\, dz \tag{2-18}$$

Substitution of Equation 2-16 into 2-18 yields

$$U = \sqrt{ghS}\left[2.5\ln\left(\frac{h}{k_r}\right) + 6.0\right] \quad (2\text{-}19)$$

where, given the assumption that the channel is wide and rectangular, R_H is taken as approximately equal to h (Hornberger et al., 1998).

The mean water velocity occurs at vertical location z_U [L], at which the velocity $u(z_U) = U$. Setting Equations 2-16 and 2-19 equal to each other and solving for the value of z_U gives

$$z_U = 0.37h \quad (2\text{-}20)$$

Hence, to measure or sample at the depth of mean velocity, experimental equipment, such as the PSFM, should be positioned at a level within the water column approximately 0.4h above the channel bed or 0.6h below the water surface (Hornberger et al., 1998).

In surface water systems that experience water level fluctuations, the absolute vertical location of any given relative depth is not fixed over time. As stream stage and total depth vary, so does the vertical positioning of average stream velocity at six-tenths relative depth. Therefore, to continuously maintain PSFM measurement at a level 0.6h below the water surface as stream stage (h) varies, the device must be deployed using the CRD apparatus. The CRD apparatus consists of a rod anchored to the streambed on one end with a float at the other end to form a right triangle with respect to the streambed and the water column, and extending the location of the PSFM intake port laterally forms a line parallel to the base of the right triangle (Figure 2-7). A line parallel to one side of a triangle and intersecting the other two sides divides these sides proportionally so that either side is to one of its segments as the other is to its corresponding segment (Hemmerling, 1964). Thus, when the PSFM intake port is positioned at a fixed relative position along the CRD apparatus float arm, it will be located in the same plane, parallel to the streambed, as a desired vertical sampling depth of the same relative position. For example, when

a float arm of length L is positioned in a stream of depth h, a PSFM intake port positioned at $0.6L$ (measured from the water surface), will also be positioned at $0.6h$, the location of mean stream velocity (Figure 2-8).

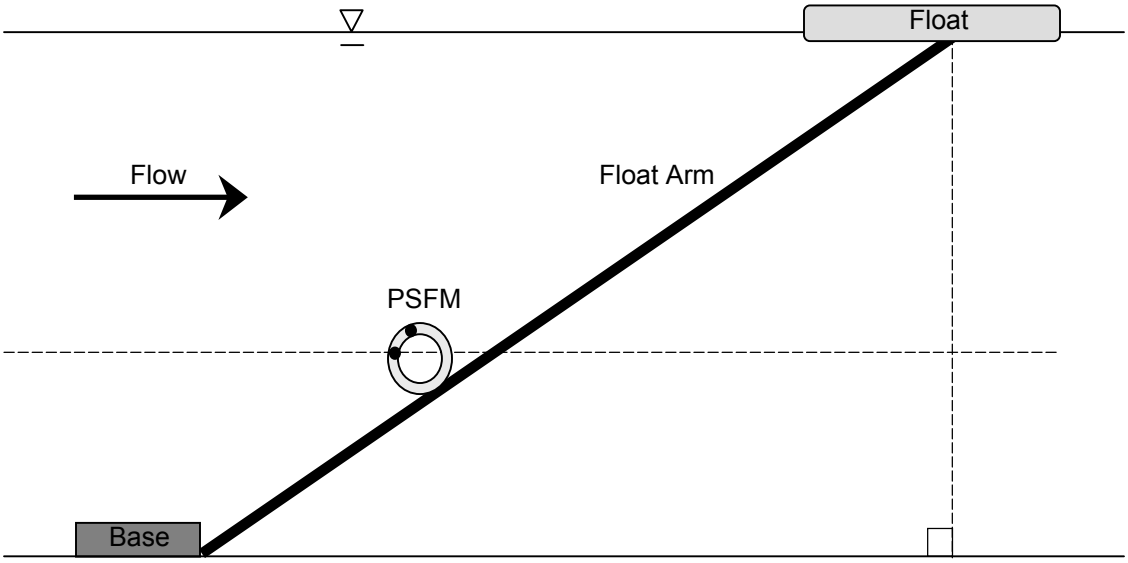

Figure 2-7. Design schematic for deployment of a cylindrical PSFM via CRD apparatus. The float arm, vertical water depth, and streambed combine to form a right triangle that is divided proportionally by the plane of the PSFM intake ports.

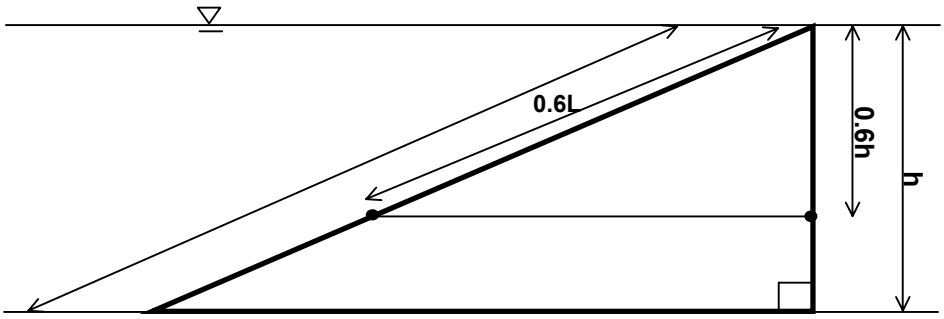

Figure 2-8. Diagram depicting the intersection of a right triangle by a line parallel to its base. It demonstrates that a point located at six-tenths the length of the hypotenuse of a right triangle is at the same vertical height as a point located at six-tenths the length of the vertical leg as measured from the water surface.

The CRD apparatus is able to sustain this measurement at six-tenths relative depth as stream stage varies (Figure 2-9). The fixed length of the float arm and the fixed position of the PSFM enable the CRD apparatus to maintain the desired geometric proportionality between the position of the PSFM along the arm and its location in reference to the vertical water column, despite any increase or decrease in water depth. Therefore, as water level fluctuates, the PSFM continuously measures at six-tenths relative depth. This has an added advantage of ensuring that the PSFM ports are never exposed to the air during period of decreased water level, which would result in desaturation of the cartridge and disruption of phosphate adsorption and tracer elution.

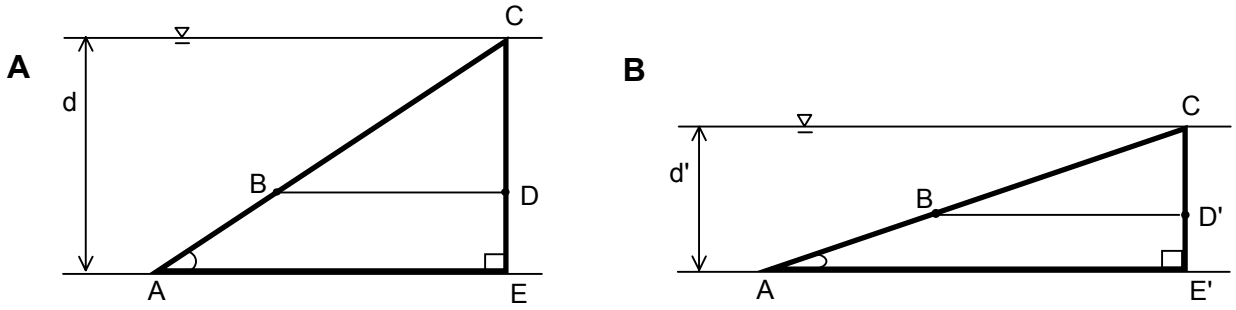

Figure 2-9. Diagram demonstrating maintenance of proportionality and constant relative depth as stream stage varies. The length of the float arm, *AC*, remains constant. The location of the PSFM cylinder, *B*, is fixed along *AC*. A) *BC* is six-tenths the length of *AC*, and *CD* is six-tenths the length of *CE*. B) As water depth, *d*, decreases to *d'*, *BC* remains six-tenths the length of *AC*, and *CD'* remains six-tenths the length of *CE'*.

2.3.2 Apparatus Design and Construction

The CRD deployment apparatus includes three basic components: base, float, and float arm. Many monitoring applications will require only a single CRD apparatus if the deployed instrumentation is sufficiently small or compact. However, larger instrumentation arrays may require multiple CRD apparatuses. The deployment of the horizontal PSFM used for flux measurement in this study required two apparatuses to support the weight of the cylinder and provide balance stabilization within the flowing stream (Figure 2-10).

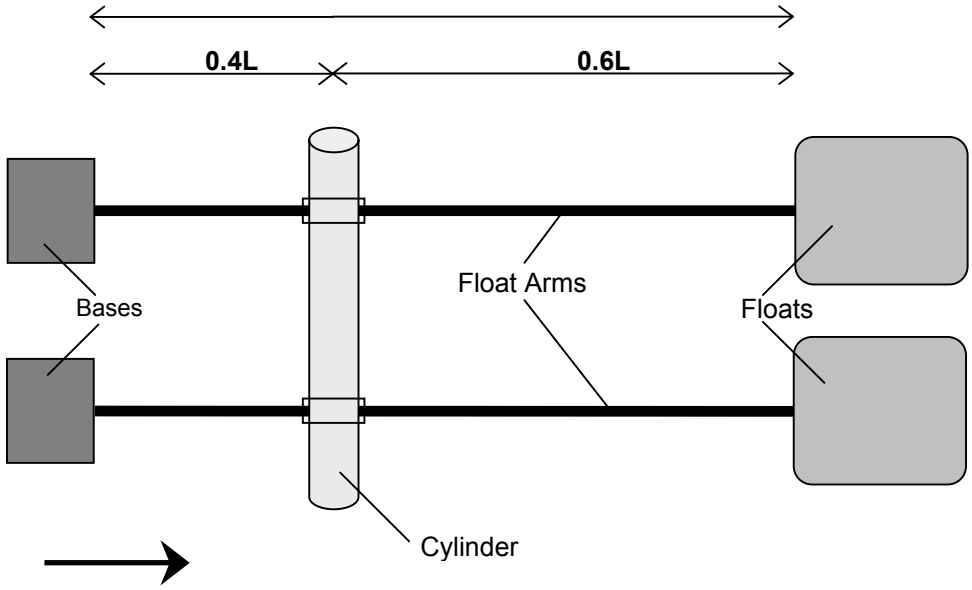

Figure 2-10. Plan view schematic of the CRD deployment apparatus. The PSFM cylinder is located at six-tenths the length of the float arms (as measured from the floats).

The CRD bases are composed of solid concrete pavers (40x40x4.5 cm), with sufficient weight to prevent downstream movement of the PSFM and CRD apparatus under normal flow conditions, and the floats are 88 cm polystyrene bodyboards. The bases connect to the floats at the water surface via the float arms, which are 153-cm long rigid 2.5-cm diameter PVC pipe. For added strength to prevent bowing of the float arms over time, the PVC was lined down the center with steel rebar. The length of the float arms was chosen based on the likely water depth range at the deployment field site. The design of the CRD apparatus allows for easy interchange of different length float arms, so that it can be easily adapted for additional field sites of different water depth. The PSFM cylinder is attached to the float arms at six-tenths the length of the float arms as measured from the water surface.

The PSFM cylinder was attached to the CRD float arms using a bead-bearings system to maintain the desired pressure-gradient-inducing port orientation within the stream flow field, even as the arms rise and fall with water level fluctuations (Figure 2-11). The system consists of

two 6-cm wide cylindrical strings of plastic craft beads (0.75 cm diameter) that loosely surround the PSFM cylinder at each end to act as bearings. The bead-bearings were hand woven on 0.38 mm nylon-coated stainless steel wire in a pattern that allows for the free rotation of each individual bead. The bearings are encompassed within outer rings that are 8 cm lengths of clear, acrylic tubing (15.25 cm OD, 14.5 cm ID), fixed directly to float arms via U-bolts. Bolts extending from the cylinder on either side of the outer rings prevent the PSFM from slipping out. As fluctuating water level changes the position of the float arms, the bead-bearings allow the bottom-weighted PSFM cylinder to rotate within the outer rings, constantly maintaining its upright position and the desired orientation of the intake and outlet ports.

Each component of the CRD deployment apparatus is transported to the field site as a separate piece. The apparatus bases, float arms, and floats are assembled in the field with zip-ties just prior to deployment, allowing for site-specific adjustments to be made relatively easily. Once the complete CRD apparatus is placed within the stream, the PSFM is positioned within the bead-bearings system, the tubing is purged and primed, the sorptive cartridges are connected to PSFM ports, and water and solute mass flux measurement can begin (Figure 2-12).

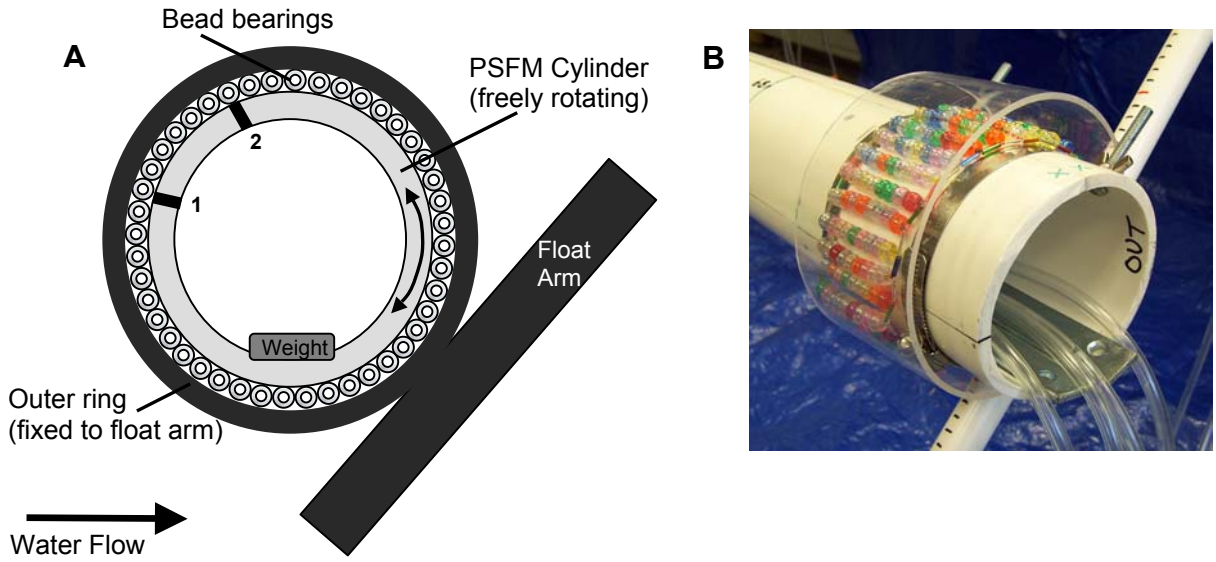

Figure 2-11. Bead-bearings system to maintain orientation of PSFM cylinder as stream stage varies. A) Design schematic of bead-bearings system. The outer ring is fixed to the float arm and separated from the PSFM cylinder by the bead-bearings. As water level fluctuations cause the float arm to change angle, the bearings allow the cylinder to rotate independently of the CRD apparatus. The weight added to the bottom of the cylinder maintains its proper orientation and port positioning within the stream flow field. B) Photograph of actual bead-bearings system constructed for field deployment.

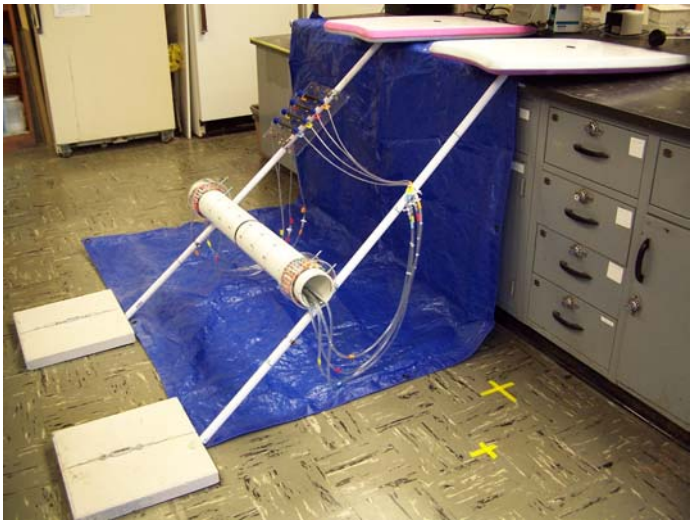

Figure 2-12. Equipment setup for field deployment of the cylindrical PSFM via CRD apparatus. At the field site, the bases are positioned on the streambed and all components of the apparatus below the floats are submerged. The PSFM is located at six-tenths the length of the float arms (as measured from the water surface) to provide continuous measurement at the vertical location of average stream velocity.

CHAPTER 3
TRACER CHARACTERIZATION

3.1 Introduction

Tracer desorption processes play an essential role in PSFM calculations for the determination of both water and solute mass fluxes. The PSFM theoretical framework requires precise knowledge of tracer retardation within the porous media and assumes tracer desorption to be instantaneous and reversible (Klammler et al., 2007). This implies that for PSFM-derived flux measurement to accurately reflect true stream conditions the chosen tracers must have known retardation factors (R_d) and must experience equilibrium desorption within the cartridge. Therefore, in order to estimate flux with a high degree of confidence, it is important to have a clear understanding of tracer behavior and characteristics within the sorptive cartridge prior to field deployment.

This study utilized laboratory tracer elution tests to determine the retardation factors of each of the following organic tracers: methanol, ethanol, isopropyl alcohol (IPA), and tert-butyl alcohol (TBA). These R_d values were subsequently employed in post-field deployment calculations to determine water and solute mass fluxes. The elution tests were also used to verify tracer mass balance and to investigate tracer desorption behavior within the cartridge through computer modeling. Model characterization of the actual tracer behavior, as compared to the theoretically assumed behavior, provided insight into the application and limitations of the tracers for PSFM flux determination.

3.2 Laboratory Tracer Elution Tests

A series of laboratory tracer elution experiments were conducted to determine the retardation of the four organic tracers used by the PSFM for flux determination. The tracers reside on the activated carbon portion of the sorptive cartridge within the PSFM device. As water

flows through the cartridge, the tracers are desorbed and eluted. Water velocity and solute mass flux are determined based on the tracer mass remaining on the activated carbon, which is directly dependent on the tracer retardation within the sorptive media. The tracer retardation factors are specifically used in Equations 2-8 and 2-10 to determine head difference across the tracer-impregnated sorptive cartridge and water velocity through the cartridge, respectively.

Elution tests also provide data to confirm mass balance of the organic tracers within the system, thus ensuring validity of PSFM flux measurements. Accurate PSFM-derived water and solute flux estimates are dependent on remaining tracer masses that are the result of purely flow-induced desorption within the cartridge. Tracer mass balance during the elution tests implies that none of the tracers are undergoing reactions other than desorption or being lost from the system via an unaccounted for process (i.e. degradation or volatilization). If mass balance does not occur during tracer elution, the PSFM measurements obtained during field deployment will not be reliable.

3.2.1 Elution Test Methods

Laboratory elution tests to determine tracer retardation factors and mass balance were conducted prior to PSFM field deployment. The suite of organic tracers monitored during the tests included methanol, ethanol, IPA, and TBA. Four long-term elution tests elution tests were conducted at cartridge flow rates of 1.7, 3.5, 5.1, and 7.5 mL/min, and two short-term elution tests were conducted at flow rates of 2.9 and 3.2 mL/min. These cartridge flow rates correspond to flow field velocities ranging from approximately 20 to 50 cm/s, as calculated using Equations 2-7 and 2-9, which are likely to be found under natural stream conditions during field deployment. The long-term tests were conducted to determine retardation of each tracer, and involved eluting as much tracer mass as possible, including complete elution (to zero mass remaining) when feasible. This allowed for more complete data sets from which to calculate R_d

values. The varying flow rates of the long-term tests were required to investigate equilibrium versus non-equilibrium tracer desorption. The short-term tests were used to confirm tracer mass balance within the sorptive cartridge and were specifically designed so that tracers would not elute completely. This allowed for tracer mass remaining to be extracted off the activated carbon for comparison to tracer mass eluted.

During each long-term test, a sorptive cartridge with tracer-impregnated activated carbon was subjected to water flow from a constant head reservoir for approximately 10 hours, during which eluent samples were collected every 10 minutes. During the short-term tests, the cartridge was subjected to flow for 45 minutes, during which eluent samples were collected approximately every 5 minutes. The desired flow rate for each test was calculated from Equation 2-9, using known values of L_c=19 cm, A=1.77 cm^2, K_c=28.8 cm/min, and ΔH across the cartridge as observed via manometers. Head differences of 0.6, 1.1, 1.2, 1.3, 1.9, and 2.8 cm generated elution test flow rates of 1.7, 2.9, 3.2, 3.5, 5.1, and 7.5 mL/min, respectively. The outflow volume was also collected during each test verify the flow rate through the cartridge and the eluted pore volumes.

After the elution period, the remaining tracer masses in each cartridge were extracted from the activated carbon via 24-hour rotation in isobutyl alcohol (IBA). All eluent and extraction samples were analyzed via Perkin-Elmer gas chromatograph (GC) with an automated liquid injection and flame ionization detector (FID) to determine tracer concentrations. These data were then used to construct plots of relative tracer mass remaining (M_r/M_i) versus eluted pore volume for each flow rate.

3.2.2 Elution Test Results

The four long-term elution tests, conducted at flow rates ranging from 1.7 to 7.5 mL/min, each produced similar tracer elution profiles (Figure 3-1). The linearity and overlap of the upper portions of the curves for a given tracer at different velocities suggests that the tracer desorption is near equilibrium at high tracer concentrations. The nonlinear tailing portions of the curves that show some variability among flow rates may be due to either differences in media packing resulting in varying dispersion characteristics (Peclet number), or some degree of desorption rate-limitation. These hypotheses were explored more closely in the subsequent modeling analyses of tracer elution.

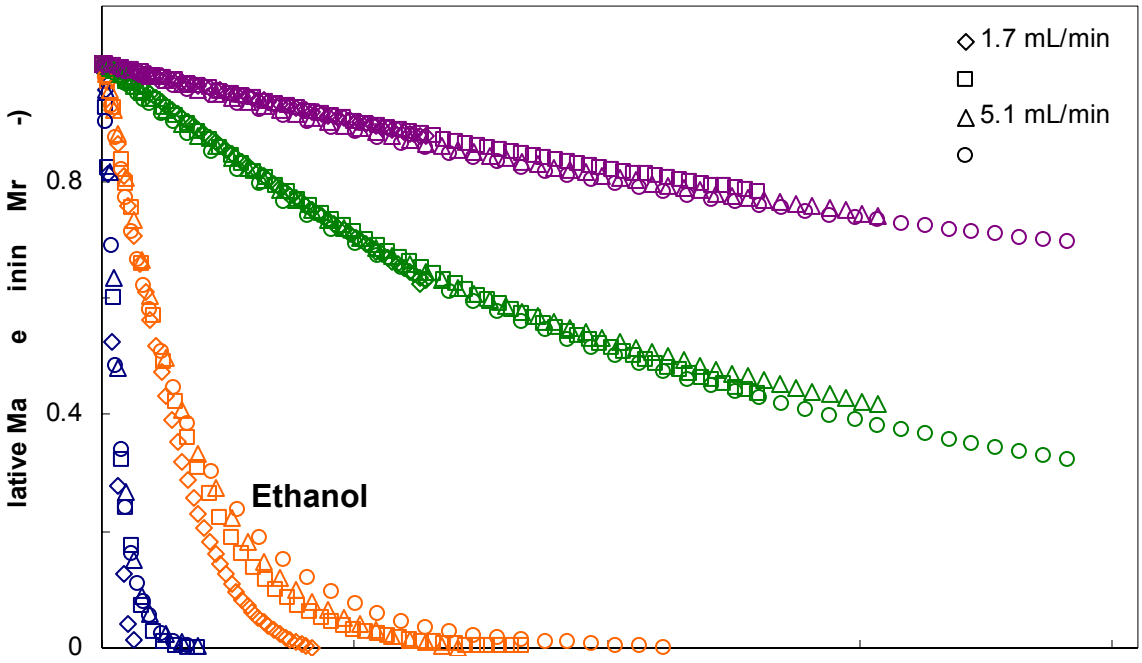

Figure 3-1. Long-term tracer elution profiles for methanol, ethanol, IPA and TBA at four flow rates.

During the long-term tests, both methanol and ethanol were eluted completely from the sorptive cartridge, while IPA and TBA were only partially eluted. Hence, these tests provided

data to confirm only the mass balances of IPA and TBA. The short-term elution tests provided data to confirm the mass balance findings for methanol and ethanol as well. The brief durations of these tests ensured that all four tracers were only partially eluted from the sorptive cartridge. For each test during which a given tracer was not entirely eluted, the percentage of mass eluted and the percentage of mass remaining on the activated carbon were summed to provide an overall mass balance (Table 3-1). On average, 97.3, 99.1, 100.3, and 98.5% of the methanol, ethanol, IPA, and TBA, respectively, were accounted for in the mass balance calculations. These findings give strong indication that there is mass balance of all the four tracers during elution.

Table 3-1 Tracer mass balance during elution at various flow rates

Tracer	Flow Rate (mL/min)	Mass Eluted	Mass Remaining	Total Mass Balance
Methanol	2.9	99.9%	2.4%	102.3%
	3.2	91.1%	1.1%	92.2%
				97.3% Average
Ethanol	2.9	35.5%	64.9%	100.4%
	3.2	37.3%	60.5%	97.8%
				99.1% Average
IPA	1.7	37.7%	63.8%	101.5%
	2.9	5.0%	100.0%	105.0%
	3.2	5.4%	99.5%	104.9%
	3.5	56.4%	38.6%	95.0%
	5.1	58.3%	35.9%	94.2%
	7.5	67.9%	33.0%	100.9%
				100.3% Average
TBA	1.7	12.4%	88.4%	100.8%
	2.9	1.8%	102.0%	103.8%
	3.2	1.9%	99.4%	101.3%
	3.5	21.9%	72.6%	94.5%
	5.1	25.8%	67.9%	93.7%
	7.5	30.5%	66.5%	97.0%
				98.5% Average

Elution profiles for each individual tracer at each of the four long-term flow rates were then combined to determine tracer retardation factors (R_d). Due to the nonlinear nature of the elution profiles, the linearization method outlined by Hatfield et al. (2004) was employed to calculate the R_d of each tracer:

$$R_d = \frac{1}{\sum_{i=1}^{p} \frac{\varphi_i - \varphi_{i+1}}{R_{di}}} \tag{3-1}$$

where R_{di} and φ_i were approximated from piece-wise linear segments of the curve (Figure 3-2). Table 3-2 lists the parameter values for each of the tracers. Methanol, ethanol, IPA, and TBA were fit with three, three, four, and two linear segments, respectively, and produced R_d values of 6.0, 23.3, 166.9, and 494.5, respectively. These R_d values compared reasonably well to those determined for the same tracers by Hatfield et al. (2004), Annable et al. (2005), and Klammler et al. (2007), with the greatest discrepancies occurring for IPA and TBA (Table 3-3). These differences in retardation may be due to variations in experimental setup, such as different sorptive media lengths or different flow rates, which are known to have effects on experimental R_d determination (Maraqa, 2001; Maraqa et al., 1999; Brusseau et al., 1991).

Had the elution curves for this study been completely linear, the tracer retardation factors would have been calculated as the reciprocals of the linear slopes. This method was applied to the upper linear portion of the elution curves for comparison to the retardation factors calculated from the piece-wise linearization method. There was little difference between the retardation factors calculated by the two methods (Table 3-4). This implies that the dispersion processes causing discrepancies among the tailing ends of the elution curves did not significantly affect tracer retardation, and that the R_d values calculated from either method are likely to produce reliable PSFM-derived flux measurements. This is especially true when the tracer mass

remaining lies in the upper, linear portion of the elution curves, which is the recommended target region (20-70% tracer mass remaining) to achieve the most accurate flux calculations (Hatfield et al., 2004). The tracer retardation factors determined via piece-wise linearization were used here for all subsequent water and solute mass flux analyses.

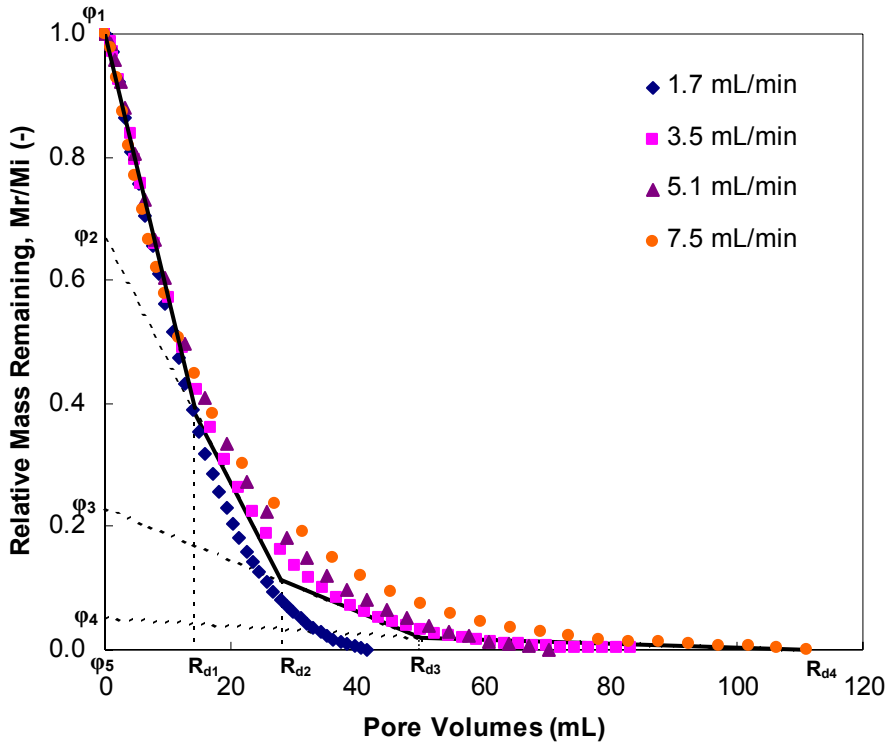

Figure 3-2. Linearization of the non-linear elution profiles of ethanol to determine tracer retardation factor. The plot combines elution data at four different flow rates and describes its linear segments via R_{di} and φ_i parameters.

Table 3-2. Retardation parameters derived from tracer elution profiles

Parameter	Tracer			
	Methanol	Ethanol	IPA	TBA
φ_1	1	1	1	1
φ_2	0.34	0.67	0.8	0.95
φ_3	0.09	0.23	0.68	0
φ_4	0	0.05	0	--
φ_5	--	0	--	--
$\varphi_1 - \varphi_2$	0.66	0.33	0.2	0.05
$\varphi_2 - \varphi_3$	0.25	0.44	0.12	0.95
$\varphi_3 - \varphi_4$	0.09	0.18	0.68	--
$\varphi_4 - \varphi_5$	--	0.05	--	--
R_{d1}	5	14	64	80
R_{d2}	8.5	28	130	680
R_{d3}	19	50	350	--
R_{d4}	--	111	--	--
R_d	**6.0**	**23.1**	**166.9**	**494.5**

Table 3-3. Inter-study comparison of tracer retardation factors

Tracer	R_d			
	Hatfield et al., 2004	Annable et al., 2005	Klammler et al., 2007	This study
Methanol	3.9	4.9	6.0	6.0
Ethanol	20.1	20.0	22.0	23.1
IPA	117.0	109.0	119.0	166.9
TBA	--	309.0	--	494.5

Table 3-4. Comparison of two methods for determining tracer retardation factors

Tracer	R_d	
	Piece-wise Linearization (entire curve)	Linear Reciprocal (upper curve only)
Methanol	6.0	5.9
Ethanol	23.1	23.2
IPA	166.9	166.6
TBA	494.5	500.0

3.3 Elution Test Modeling

Measured laboratory elution breakthrough curves (BTCs) for each of the four tracers were modeled with the advection dispersion equation (ADE) with consideration of both equilibrium and non-equilibrium sorption. The ADE was solved numerically using HYDRUS-1D (Simunek et al., 2005). This software was selected because of its relative ease of use. Fitting the experimental BTCs to modeled desorption curves allowed for the investigation of sorption reactions within the PSFM cartridge, as well as the determination of unknown parameters controlling solute transport. These parameters, namely dispersivity, help to characterize the sorption reactions, providing insight into conditions that the tracers are experiencing during elution and the processes that are controlling variations in curve tail.

The ADE for solute transport one-dimensional variably saturated media is given by (Simunek et al., 2005)

$$\frac{\partial R_d \theta C}{\partial t} = \frac{\partial}{\partial x}\left(\theta D \frac{\partial C}{\partial x}\right) - \frac{\partial v \theta C}{\partial x} \tag{3-3}$$

where C [ML^{-3}] is the solute concentration, D [L^2T^{-1}] is the effective dispersion coefficient, and v [LT^{-1}] is the pore water velocity. The retardation factor, R_d, and dispersion coefficient, D, are defined as (Simunek et al., 2005)

$$R_d = 1 + \frac{\rho_b K_d}{\theta} \tag{3-4}$$

$$D = \lambda |v| \tag{3-5}$$

where K_d [L^3M^{-1}] is the linear adsorption distribution coefficient, ρ_b [ML^{-1}] is the bulk density, and λ [L] is the longitudinal dispersivity. Equation 3-5 assumes that molecular diffusion is insignificant relative to dispersion (Inoue et al., 2000).

3.3.1 Model Inputs and Methods

The four long-term elution tests, conducted at flow rates of 1.7, 3.5, 5.1, and 7.5 mL/min, were chosen for HYDRUS-1D general solute transport simulation under the above conditions. Given that HYDRUS-1D is a one-dimensional modeling program, these cartridge flow rates were converted to water velocities of 0.96, 2.0, 2.9, and 4.2 cm/min, respectively. The initial condition for each elution simulation was obtained by establishing steady-state flow and constant solute flux. The head differences necessary to produce the desired flow velocities, 0.86, 1.76, 2.57, and 3.78 cm, respectively, were calculated using Equation 2-9 and the previously determined K_c=28.8 cm/min. Other porous medium hydraulic input parameters included θ=0.55 and one-dimensional ρ=1168 mg/cm, which had been previously determined in the laboratory. The profile length was input as the length of only the activated carbon portion of the cartridge (L=14.5 cm), as this is the material that experiences tracer desorption. For all simulations, linear sorption was assumed.

The upper boundary condition for solute transport (at the sorptive media surface, x=L) was described as concentration flux, and is given by (Simunek et al., 2005)

$$-\theta D\frac{\partial C}{\partial x}+qC=q_oC_o \tag{3-6}$$

where q_o [LT-1] is the fluid flux at the surface and C_o [ML-3] is the solute concentration of the incoming fluid. A zero concentration gradient was used as the lower boundary condition for solute transport (at x=0), and is given by (Simunek et al., 2005)

$$\left(\frac{\partial C}{\partial x}\right)_{x=0}=0 \tag{3-7}$$

Within HYDRUS-1D, the initial sorbed concentration is determined using the input of the initial solute concentration in solution and the equilibrium sorption model, given by the equilibrium isotherm (Simunek et al., 2005)

$$S = K_d C \tag{3-8}$$

where S [MM^{-1}] is initial sorbed concentration. Sorption coefficients (K_d) for each separate tracer were calculated via Equation 3-4 using the laboratory-determined retardation factors, water content, and one-dimensional bulk density, and initial sorbed tracer concentrations were determined by extraction from uneluted tracer-impregnated activated carbon (Table 3-5). These values were then used in Equation 3-8 to calculate the appropriate initial solute concentration input values for each tracer.

Table 3-5. Solute transport parameters for elution test modeling

Tracer	K_d (cm^3/mg)	S (mg/mg)	C (mg/cm^3)
Methanol	0.0041	0.002	0.50
Ethanol	0.0185	0.002	0.11
IPA	0.1383	0.004	0.03
TBA	0.4158	0.004	0.01

The experimental elution data for each tracer at each flow rate were also input into HYDRUS-1D so that the program could generate R^2 values for statistical comparison between the experimental data and modeled fit. The R^2 value is a measure of the relative magnitude of the total sum of squares associated with the fitted equation, and is given by (Simunek et al., 2005)

$$R^2 = \frac{\left[\sum w_i x_i y_i - \frac{\sum x_i \sum y_i}{\sum w_i}\right]^2}{\left[\sum w_i x_i^2 - \frac{\left(\sum x_i\right)^2}{\sum w_i}\right]\left[\sum y_i^2 - \frac{\left(\sum y_i\right)^2}{\sum w_i}\right]} \tag{3-9}$$

where x_i is the observed value, y_i is the fitted value, and w_i is the weighting factor assigned to a given data point. For this study, all experimental data points were given equal weight.

All tracers were initially fit in accordance with PSFM theory using the equilibrium sorption model. It was hypothesized that if the tracers were undergoing the assumed equilibrium desorption, differences in late-time tailing between experiments would be due to differences in the dispersive characteristics of the sorptive cartridge used in each elution test, rather than rate-limitation of tracer desorption that would imply non-equilibrium. When experiencing equilibrium desorption, the upper, linear portion of an elution curve is controlled by the retardation of a given tracer, while the lower, curved portion is controlled by the dispersive characteristics of the porous medium. Slight differences in dispersivity of the activated carbon within each sorptive cartridge are likely to develop, because it is difficult to exactly duplicate the packing of each cartridge, and variations in dispersivity would be expressed as a different Peclet number (P [-], ratio of advection to dispersion) for each sorptive cartridge. Hence, if each of the four elution experiments for a given tracer could be fit with the same R_d, but different P, there would be good indication that the variations in curve tailings are due to differences in the packing of the activated carbon and not rate-limitation resulting from varying flow velocity.

Because dispersivity is considered a porous media property rather than a solute property, the same dispersivity was assumed for all tracers that were eluted from each sorptive cartridge. Dispersivity in each packing was determined from best fits of the equilibrium ADE to the BTCs for methanol, the least reactive of the resident tracers. These dispersivities were then used to calculate P for each velocity experiment and used to predict behavior of the remaining three tracers within the model.

The potential for rate-limited sorption was subsequently investigated using the two-site sorption model within HYDRUS-1D. The two-site model allows for the consideration of non-equilibrium sorption reactions and assumes that sorption sites can be divided into two fractions:

type-1 sites that experience instantaneous sorption and type-2 sites that experience time-dependant sorption governed by a first-order kinetic rate process. The dimensionless governing equations for the two-site model are given by (Simunek et al., 2005)

$$\beta R_d \frac{\partial C^*}{\partial T} + (1-\beta) R_d \frac{\partial S^*}{\partial T} = \frac{1}{P}\frac{\partial^2 C^*}{\partial X^2} - \frac{\partial C^*}{\partial X} \tag{3-10}$$

$$(1-\beta) R_d \frac{\partial S^*}{\partial T} = \omega (C^* - S^*) \tag{3-11}$$

where,

$$X = x/L \tag{3-12a}$$

$$T = v_o t/L \tag{3-12b}$$

$$C^* = C/C_o \tag{3-12c}$$

$$S^* = \frac{1}{(1-F)K_d}\frac{S_2}{C_o} \tag{3-12d}$$

$$P = v_o L/D \tag{3-12e}$$

$$\beta = \frac{\theta + F\rho K_d}{\theta + \rho K_d} \tag{3-12f}$$

$$\omega = \frac{k_2 L}{v_o}(1-\beta) R_d \tag{3-12g}$$

where D [L^2T^{-1}] is the dispersion coefficient, S_2 [MM^{-1}] is the average sorbed concentration in the rate-limited domain, F [-] is the fraction of sites for which sorption is instantaneous, k_2 [T^{-1}] is the first-order rate coefficient applied to type-2 sorption sites, β [-] is the fraction of instantaneous retardation, and ω [-] is the Damköhler number (ratio of hydrodynamic residence time to characteristic time for sorption).

3.3.2 Model Results

The modeled best-fits for equilibrium methanol desorption determined dispersivities for the 0.96, 2.0, 2.9, and 4.2 cm/min simulations to be 9.4, 12.1, 4.6, and 10.5 cm^{-1}, respectively, which produce *P* values of 1.54, 1.20, 3.16, and 1.38, respectively. These very low *P* values indicate that the activated carbon is a highly dispersive porous medium. This is likely due to the extremely jagged surface structure of activated carbon grains, which provides many alternate pathways for solute transport, thus enhancing and promoting high differential advection (dispersion).

Applying the methanol-derived dispersivities to the remaining three tracers generated predictions that fit very well for all ethanol simulations, reasonably well for all IPA simulations, and reasonably well for lower velocity TBA simulations (R^2 values reported in Table 3-6). Hence, the variations in dispersive characteristics between experimental cartridges and the goodness of fit to the equilibrium desorption model indicate that the differences in elution curves can be partially explained by variations in cartridge packing. However, equilibrium predictions for the higher velocity simulations of both IPA and TBA did not generate fits with the same degree of goodness (lower R^2 values), which would indicate some rate-limitation of these tracers at higher cartridge velocities.

To investigate this apparent non-equilibrium behavior, each of the four velocity simulations for IPA and TBA was individually best-fit for *F* and k_2 parameters using the two-site model (Table 3-6). While the model theory assumes a constant k_2 that does not vary with flow velocity, a correlation between k_2 and velocity has been observed in several studies (Maraqa, 2001; Maraqa et al., 1999; Kookana et al., 1993; Brusseau, 1992; Brusseau et al., 1991). Variations in *F* with flow velocity have also been reported (Kookana et al., 1993). Similar variations with velocity were determined to also occur in this study, because the individual best-

fits, among which k_2 and F varied, generated the most accurate predictions of experimental elution. This was established by contrasting the best-fits for each tracer to simulations made using parameters derived from the most rate-limited simulation (4.2 cm/min) (Figure 3-3). The comparison demonstrated that for each given tracer, elution at varying velocities could not be described using the same values of k_2 and F. Hence, these parameters were concluded to be velocity dependant.

Table 3-6. Parameters for equilibrium and rate-limited tracer elution modeled in HYDRUS-1D

		Equilibrium		Rate-limited		
Tracer	Velocity (cm/min)	P	R^2	F	k_2 (1/min)	R^2
Methanol	1.7	1.54	0.9764			
	3.5	1.20	0.9634			
	5.1	3.16	0.9932			
	7.5	1.38	0.9679			
Ethanol	1.7	1.54	0.9701			
	3.5	1.20	0.9974			
	5.1	3.16	0.9940			
	7.5	1.38	0.9807			
IPA	1.7	1.54	0.9590	--	--	--
	3.5	1.20	0.9918	0.74	0.0011	0.9962
	5.1	3.16	0.9195	0.69	0.0021	0.9958
	7.5	1.38	0.9397	0.56	0.0036	0.9855
TBA	1.7	1.54	0.9612	--	--	--
	3.5	1.20	0.9266	0.59	0.0002	0.9787
	5.1	3.16	0.7320	0.49	0.0006	0.9824
	7.5	1.38	0.7969	0.34	0.0008	0.9766

Comparing the R^2 values demonstrates that the non-equilibrium two-site sorption model with velocity dependant parameters provides a better fit to the experimental elution data for IPA and TBA than the equilibrium model at velocities of 2.0, 2.9, and 4.2 cm/min (Table 3-6). At 0.96 cm/min, both tracers experience desorption that is at equilibrium, but with increasing

velocity, F decreases and k_2 increases. The decrease in F indicates that not all reaction sites along the jagged activated carbon surface are accessible at a given flow rate, with fewer and fewer equilibrium sites being reached by tracer solutes as velocity increases (Kookana et al., 1993). Further, the increase in k_2 indicates that as velocity increases the type-2 sorption reactions are also becoming more rate-limited. This is likely to occur as a result of slow solute diffusion, which limits the ability of tracers to desorb at higher flow velocities. Hence, it appears that both physical and chemical processes are contributing to the observed non-equilibrium desorption of IPA and TBA. The HYDRUS-1D elution simulations are able to capture the effects of both types of processes, because physical (mobile-immobile) and chemical (two-site) non-equilibrium models are mathematically equivalent (Nkedi-Kizza et al., 1984).

There was also a relationship observed between tracer reactivity and degree of rate-limitation. When comparing IPA (K_d=0.1383) and TBA (K_d=0.4158), as tracer reactivity (retardation) increases, k_2 decreases (Table 3-6). Lower k_2 values indicate slower sorption reaction rates, implying that the reaction is more rate-limited. Hence, more reactive tracers experience a greater degree of rate-limitation during sorption.

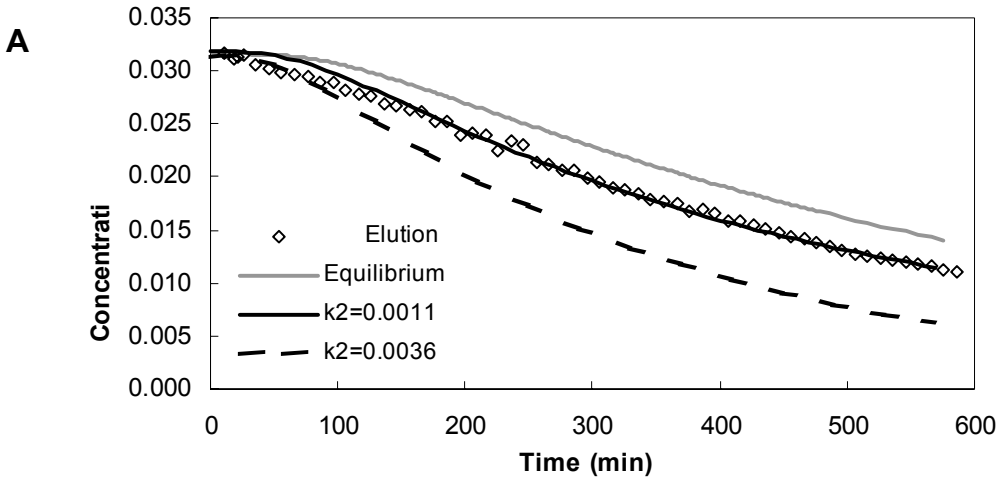

Figure 3-3. Comparison of three predictions for tracer desorption. Blue lines represent equilibrium desorption, red lines are best-fit rate-limited desorption, and yellow lines

are rate-limited desorption derived from 4.2 cm/min simulation parameters. A) IPA simulations at 2.0 cm/min. B) TBA simulations at 2.0 cm/min.

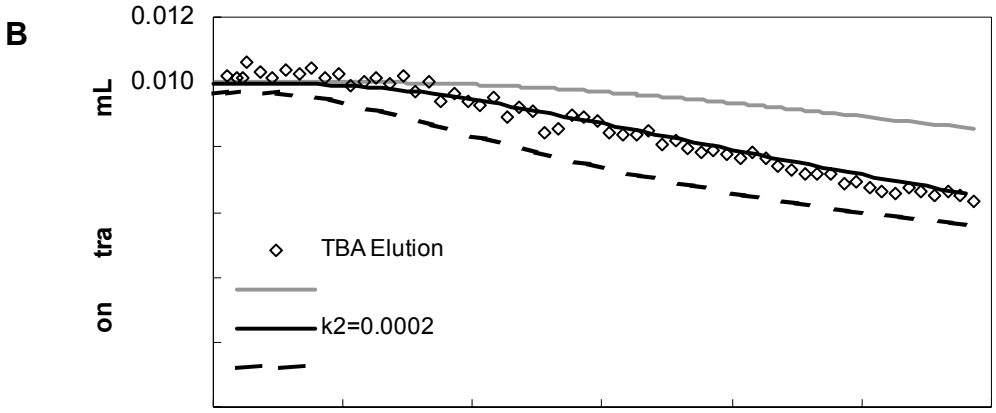

Figure 3-3. Continued.

3.3.3. Modeling Implications

The modeling results showed that while methanol and ethanol experience equilibrium desorption within the PSFM sorptive cartridge, IPA and TBA are better characterized by velocity-dependent rate-limited desorption (Figure 3-4). In previous flux meter studies, tracer elution was characterized using a linear, one-parameter (R_d) model that assumed equilibrium desorption and the dominance of advection (Klammler et al., 2007; Alvarez et al., 2005; Padowski, 2005; Hatfield et al., 2004). Application of this one-parameter model to nonlinear elution curves prevented the use of the tracers for flux determination below approximately 20% mass remaining, because beyond this level laboratory elution curves deviated from the model (Figure 3-5A). The HYDRUS-1D two-parameter model (R_d, P) incorporated by this study has advantages to the one-parameter model when using tracers that experience equilibrium desorption within the highly dispersive porous medium. By incorporating varying dispersivity, equilibrium tracer elution can be well fit over the entire length of the profiles (Figure 3-5B). This eliminates the need for a target level of tracer mass remaining. If the two-parameter model is

incorporated into PSFM theory, methanol and ethanol could be used for flux determination up until zero mass remaining with a relatively high degree of confidence. However, the two-parameter model is still not sufficient for characterizing IPA and TBA, tracers that experience non-equilibrium desorption within the sorptive cartridge.

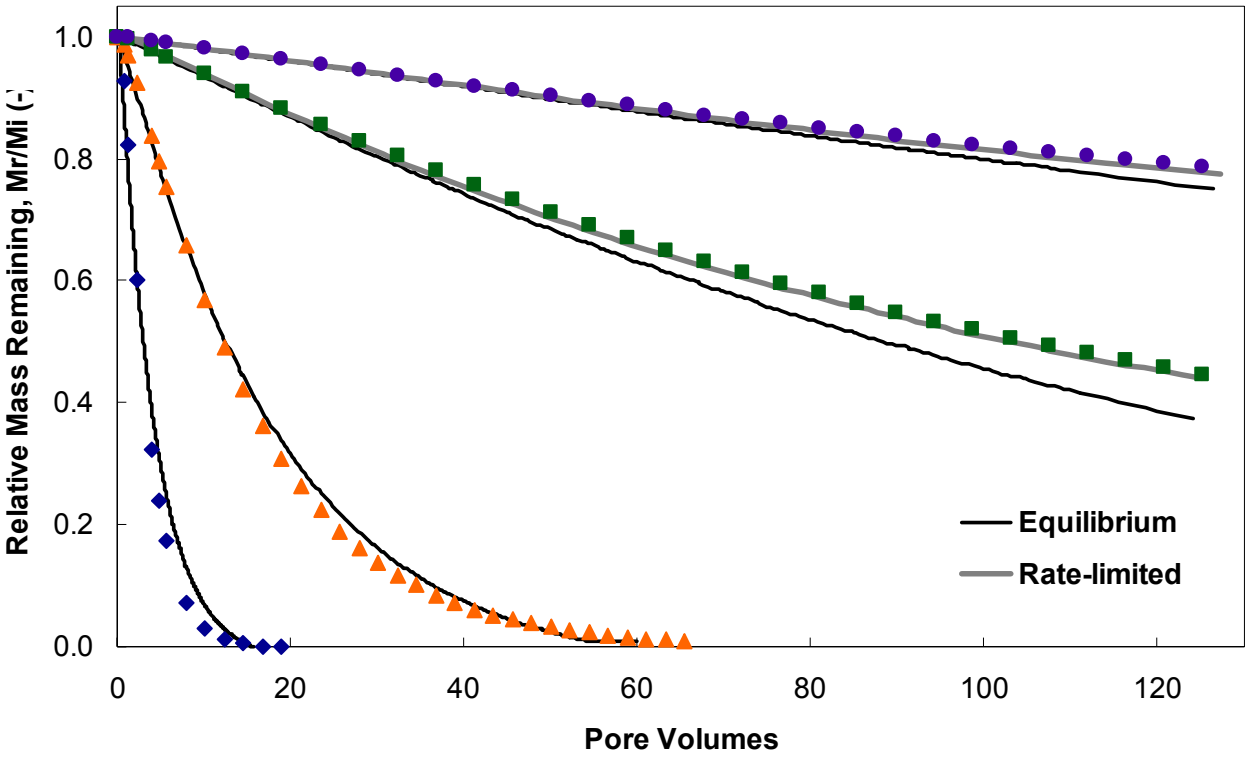

Figure 3-4. Experimental and modeled elution profiles for methanol, ethanol, IPA, and TBA at 2.0 cm/min. Methanol and ethanol are both well approximated by the equilibrium desorption model, while IPA and TBA are better approximated by the rate-limited two-site desorption model.

Fitting the laboratory elution curves for IPA and TBA required the use of a HYDRUS-1D non-equilibrium, four-parameter model (R_d, P, k_2, F). The evidence of the rate-limited sorption for IPA and TBA has implications for both deployment duration and stream velocity when using these tracers for flux determination. The deviation of non-equilibrium rate-limited sorption from equilibrium behavior increases with increased deployment duration for both tracers (Figure 3-6). This deviation does not occur until later in the elution profile for IPA, but it occurs early and to a

greater degree for TBA. At some point the rate-limited curves begin to experience decreases in relative mass remaining that occur at extremely small increments. This happens because as the tracers elute and the sorbed concentrations decrease, there is less of a diffusive gradient between the sorbed and aqueous phases. As a result, the rate of tracer desorption off the activated carbon decreases exponentially. This implies that for extended deployment durations, tracer mass remaining remains relatively constant with time, making accurate flux determination difficult. Further, since the tracers experience rate-limitation that increases with cartridge flow rate, the departure from equilibrium behavior will be even more pronounced at higher stream velocities.

Given that this study was focused on relatively short term field-testing of the PSFM, generally within the equilibrium-approximated ranges for all tracers, it is unlikely that the observed rate-limitation will have significant effects on accurate flux determination. However, the use of IPA and TBA as PSFM resident tracers for flux measurement during temporally extended field deployments should be carefully considered using the following guidelines:

- At mass remaining greater than 50% for IPA and greater than 80% for TBA, there is less than 10% error between the equilibrium and non-equilibrium models. Hence, both tracers should be relatively accurate flux predictors according to the equilibrium model within these ranges.

- For IPA, mass remaining values of 0-50% exhibit 10-40% error between the equilibrium and non-equilibrium models. For TBA, mass reaming values of 45-80% exhibit 10-60% error between the equilibrium and non-equilibrium models. Within these ranges it is necessary to incorporate the four-parameter rate-limited model to accurately determine water and solute fluxes.

- Below 45% mass remaining, TBA should no longer be used for flux determination. The non-equilibrium model demonstrates that after 45% the mass remaining decreases at a very slow rate, making the relationship between tracer mass and pore volume difficult to accurately predict. To successfully deploy the PSFM for longer durations would require a flow rate at which the tracers experience equilibrium desorption within the cartridge (below 1.7 cm/min). Achieving such an equilibrium flow rate is possible by either deploying at stream velocities less than 20 cm/s, or by using a finer porous medium to decrease the hydraulic conductivity of the sorptive cartridge.

The mass remaining values reported in these criteria are based on the extended simulation of the 3.5 mL/min elution test (Figure 3-6), which corresponds to a stream velocity of 30 cm/s, the approximate field velocity encountered in the field-testing portion of this study. However, modeling the extended tracer elution at other cartridge flow rates can develop specific criteria for other stream velocities.

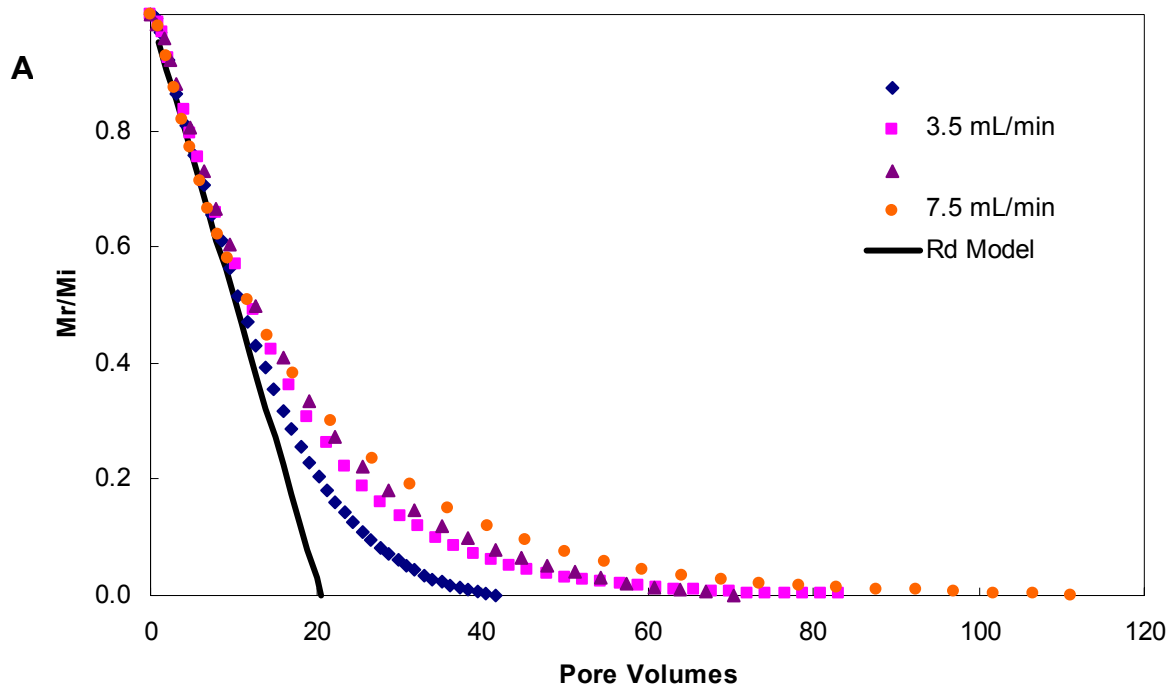

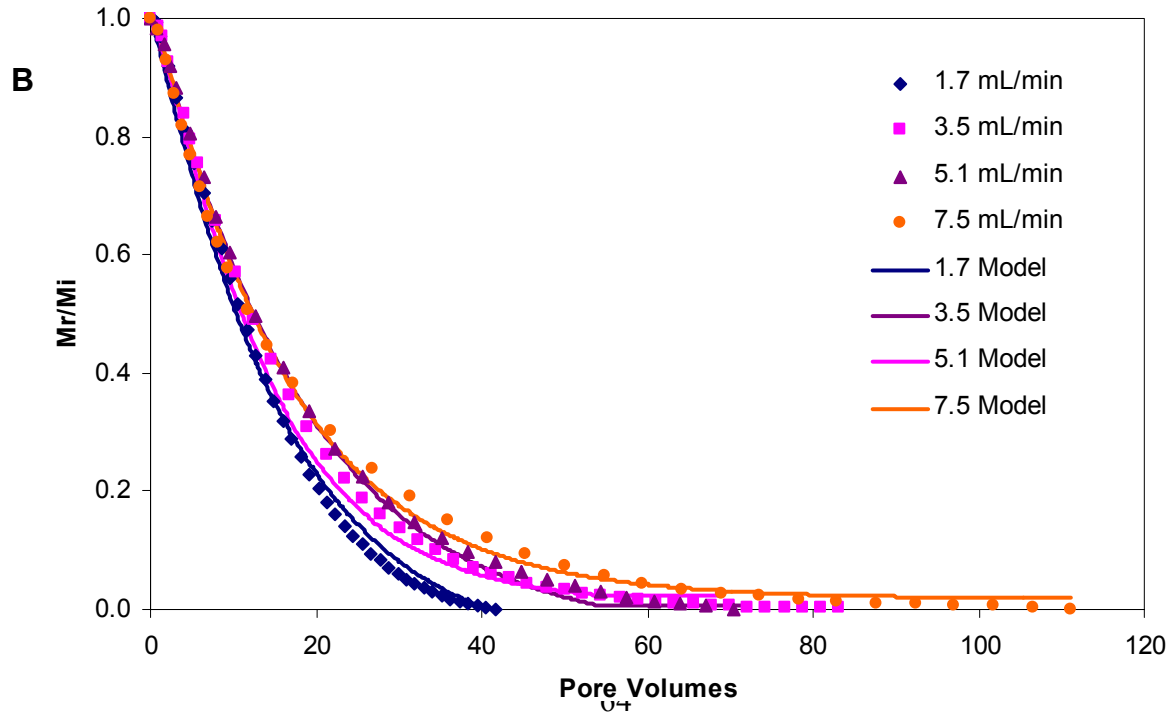

Figure 3-5. Ethanol elution curves fit with alternate equilibrium models. A) Traditional, one-parameter (R_d) model. B) HYDRUS-1D two-parameter (R_d, P) model.

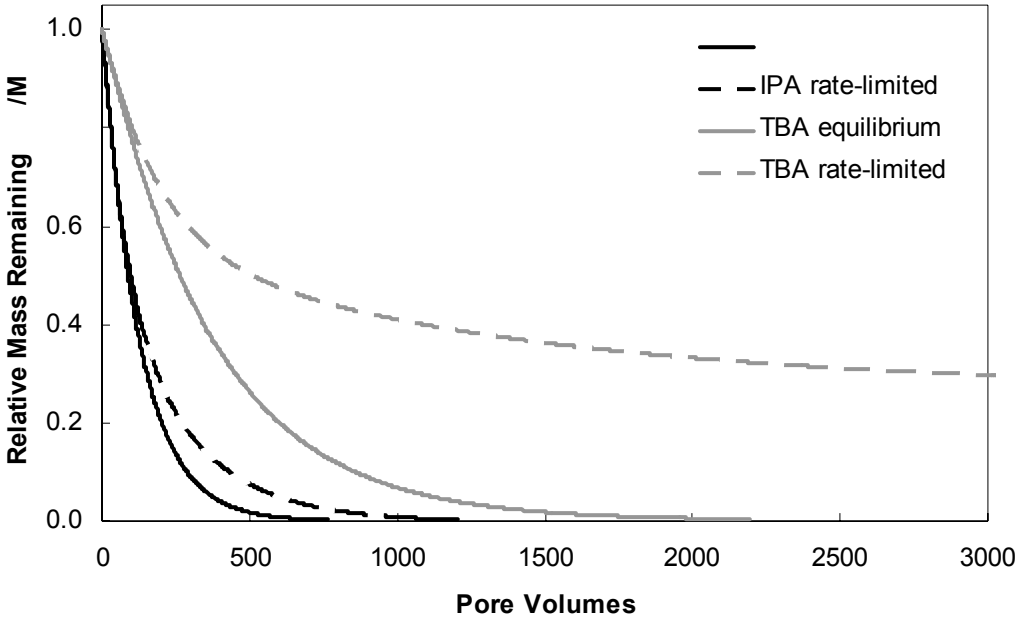

Figure 3-6. Extended simulations of IPA and TBA elution at 2.0 cm/min (3.5 mL/min) as modeled by HYDRUS-1D. As relative mass remaining decreases, deviations between the equilibrium and rate-limited sorption models increase.

CHAPTER 4
STEADY-STATE FIELD DEPLOYMENT

4.1 Introduction

The first step in demonstrating the applicability of the PSFM for a variety of water resources applications is validating its accuracy for determining water and solute mass fluxes under steady-state conditions. Given the previous success of the device in steady-state laboratory settings, field-testing within natural flowing surface bodies was the logical next progression in the PSFM development process. The stream locality chosen by this study for initial field-testing had predictable water flows and elevated nutrient levels, where conditions were assumed to be at steady state over limited durations. The PSFM was deployed for flux measurement with the CRD apparatus, which allowed for concurrent testing of the fundamental performance and compatibility of the two technologies.

4.2 Deployment Site Description

Several criteria were considered in choosing an appropriate field site for deployment of the PSFM and CRD apparatus. Water depth should be between approximately 0.5 and 1.5 m. Levels below 0.5 m could interfere with the mechanisms of the CRD apparatus and result in PSFM port exposure, while levels above 1.5 m would not allow a person to position and adjust the PSFM and CRD while standing (with head above water) within the stream. Water velocity should be between 25 and 65 cm/s, corresponding to the velocity range that has been successfully tested in the flume. The flow conditions should be as constant as possible over short durations so that the steady-state flux equations are applicable, but should also have the potential to produce variable flow conditions for eventual transient testing. Suspended solids within the water body should be relatively low to avoid interference and clogging within the tubing and sorptive column. The

field site should also be easily accessible so that all equipment can be easily transported, but relatively secluded so that experiments are not disturbed.

A location within Sweetwater Branch, an urbanized creek draining a 3.3 square-mile watershed in central Gainesville, FL, was chosen as the first PSFM field deployment site (Figure 4-1). The site was selected due to its downstream location from a water reclamation facility that discharges 5.5 to 7.5 million gallons per day into the creek (RPG, 2003). This relatively continuous discharge of treated municipal wastewater was expected to maintain steady, predictable stream flows, elevated nutrient levels, and low suspended solids, thus generating significant water and solute mass fluxes for PSFM determination.

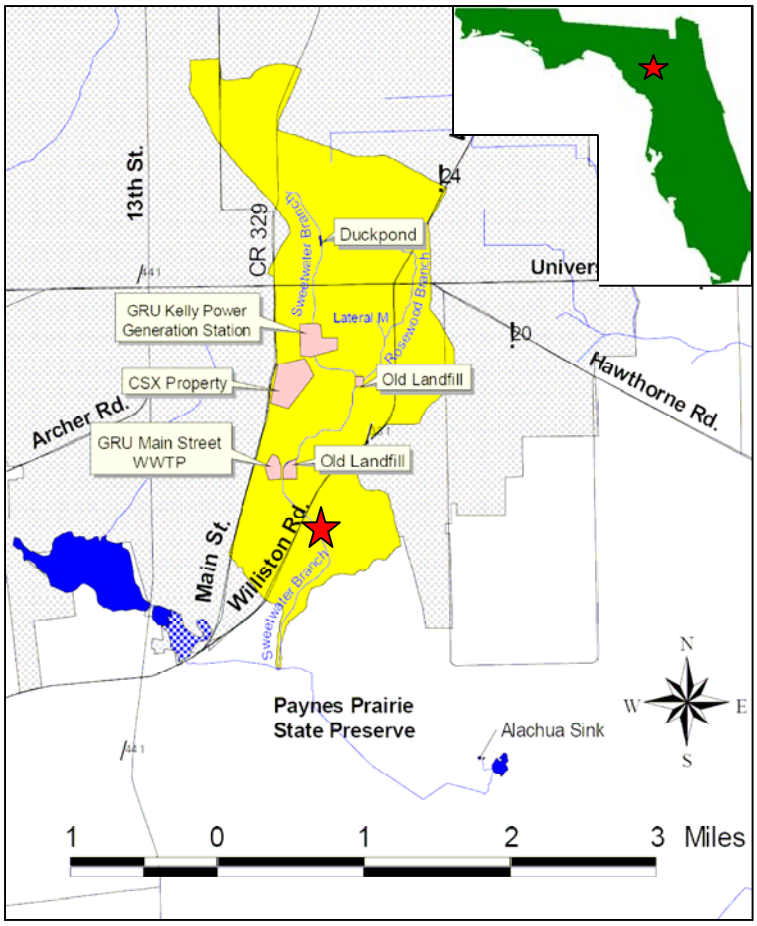

Figure 4-1. Location and watershed delineation of PSFM field deployment site in Sweetwater Branch, Gainesville, FL. (Adapted from RPG, 2003)

Sweetwater Branch is part of the larger-scale Orange Creek Basin, and flows through the Northern and Central Highland physiographic provinces of north-central Florida. Its headwaters are located in northwest Gainesville, where they have been channelized and exist as baseflow in underground concrete culverts of the municipal stormwater system. The creek's visible surface flow begins near the intersection of Main Street and NW 16th Avenue, where it flows south through the heart of the downtown area. It continues on a general southerly route, flowing through an industrial area where it receives non-contact cooling water discharged from the Gainesville Regional Utility (GRU) J.R. Kelly Electrical Power Generating Station and treated municipal effluent from the GRU Main Street Water Reclamation Facility (WRF). Sweetwater Branch then flows into Paynes Prairie State Preserve where it ultimately discharges to the Floridian Aquifer via the Alachua Sink. Approximately 90% of the watershed is highly developed for urban, industrial and residential land uses and contains significant amounts of impervious surface (RPG, 2003).

Sweetwater Branch is currently experiencing elevated levels of nitrogen and phosphorus. The Florida Department of Environmental Protection (2006a) determined nitrogen to be the limiting nutrient within the system and subsequently developed a total nitrogen (TN) TMDL for Alachua Sink that included TN limitations for Sweetwater Branch. However, since this project studies phosphate as the solute of interested for PSFM flux determination, attention will be focused on previously reported phosphorus levels within the creek. From 2000 to 2004, the total phosphorous (TP) loading conveyed through Sweetwater Branch was estimated at an average of 19,224 pounds per year (FDEP, 2006a). In 2002, the mean baseflow TP concentration south of the GRU Water Reclamation Facility was 1.11 mg/L, with a maximum single baseflow TP concentration of 5.94 mg/L, however the sample counts and frequencies of these data were not

reported (RPG, 2003). Over the course of the field-testing campaign of this study (January to May 2007), five (approximately monthly) grab sampling episodes of three replicates each indicated that baseflow TP concentrations within the creek ranged from 2.4 to 7.7 mg/L, with an average of 4.0 ± 1.8 mg/L.

The elevated phosphorus levels in Sweetwater Branch are the result of several potential loading pathways, including both point and nonpoint sources. The most obvious point source is the Main Street WRF discharge. It is estimated that the WRF contributes 59.5% of the annual TP load within the creek (FDEP, 2006a). While the discharge is wastewater that has been treated for nutrient reduction, residual levels within the effluent are still high enough to elevate overall phosphate concentrations within Sweetwater Branch, especially considering that the effluent makes up a majority of the continuous baseflow of the once intermittent creek. The WRF discharge may also be contributing to elevated phosphorus levels in an indirect manner as well. Given that flow within Sweetwater Branch is currently 14 times higher than what it would be without the WTF discharge, it is possible that the stream bank incising caused by this significantly increased volume of water may be cutting down through the phosphatic minerals of the underlying Hawthorne Group, resulting in additional releases of phosphorus into the water column (FDEP, 2006a; RPG, 2003).

Nonpoint sources of phosphorus loading to Sweetwater Branch include poor stormwater management and leaking septic systems within the watershed. The high degree of developed, impervious surfaces and the lack of a stormwater management system allow for direct discharges of non-treated stormwater into the creek. Further, the majority of the watershed lacks adequate riparian buffers that would attenuate rate, volume, and quality of stormwater (RPG, 2003). Septic tank leakage has also been identified as a potential phosphorus source due to elevated fecal

coliform bacteria levels within Sweetwater Branch, and it is estimated that septic tanks contribute 11.2% of the annual TP load within the creek (FDEP, 2006a; RPG, 2003).

While increased flows and nutrient levels have resulted in some impairment of Sweetwater Branch, these conditions also make it an ideal test site for PSFM monitoring. The specific deployment site for this study (29.63°, -82.32°) was located in Sweetwater Branch south of the intersection of SE 16th Avenue (SR 226) and Williston Road (SR 331), immediately after the creek passes under Williston Road through a double-box culvert (Figure 4-2). This region is downstream of the WRF discharge location, and thus experiences continuous stream flow and elevated nutrient levels under normal conditions. At the position chosen for PSFM deployment, the creek maintains baseflow conditions of width, depth, and velocity at approximately 3.5 m, 65 cm, and 30 cm/s, respectively. The site has a small stretch of level, sandy shoreline that provides workspace for assembling deployment equipment and allows for easy access to the creek for PSFM positioning and associated monitoring activities. There is also a St. Johns River Water Management District (SJRWMD) stream stage and discharge monitoring station (#01980199) located within 50 meters of the deployment site, which could provide additional data for comparison to PSFM-derived measurements.

Figure 4-2. PSFM deployment site in Sweetwater Branch. The site is located adjacent to the intersection of SE 16th Avenue and Williston Road in Gainesville, FL.

4.3 Field Deployment Methods

In preparation for field deployment, all sorptive cartridges were packed in the laboratory prior to travel to the field site. At the field site, the PSFM and CRD apparatus were assembled and positioned within the creek, normal to the direction of stream flow (Figure 4-3). The horizontal positioning of the PSFM device, with four port pairs located at six-tenths relative depth, allowed for replicate sampling via four simultaneously operated sorptive cartridges. Once the cartridges had begun flux measurement, dye was injected into tubing at the outflow ends to visually confirm flow and obtain estimates of water velocity through the cartridges. One or two sets of replicate sampling trials were performed during each field excursion, depending on the time constraints of the tracer mass remaining predictions, which were largely contingent on the particular tracer of interest and stream velocity. Over the course of the study, five steady-state deployment experiments were conducted with durations between 40 and 495 minutes.

Figure 4-3. The PSFM and CRD apparatus deployed within Sweetwater Branch under steady-state flux conditions.

At the outset of each steady-state PSFM deployment, water velocity and solute concentration were independently measured for use in calculations of true water and solute fluxes. These true flux values would subsequently be used to determine the accuracy of PSFM-derived estimates. Velocity measurements were made using an acoustic Doppler velocimeter (SonTek FlowTracker) and standard stream gauging methodology (BOR, 2001), with measurements taken at relative depths of 0.2, 0.6, 0.8, and 1.0 at five lateral locations across the width of the creek (Figure 4-4). Water velocities at each individual PSFM intake port where then interpolated from this cross-sectional array of profiles. Replicate grab samples were collected for laboratory analysis of TP concentration within the stream flow. The PSFM intake port depths were also measured to confirm the CRD apparatus positioning of the device at six-tenths relative depth.

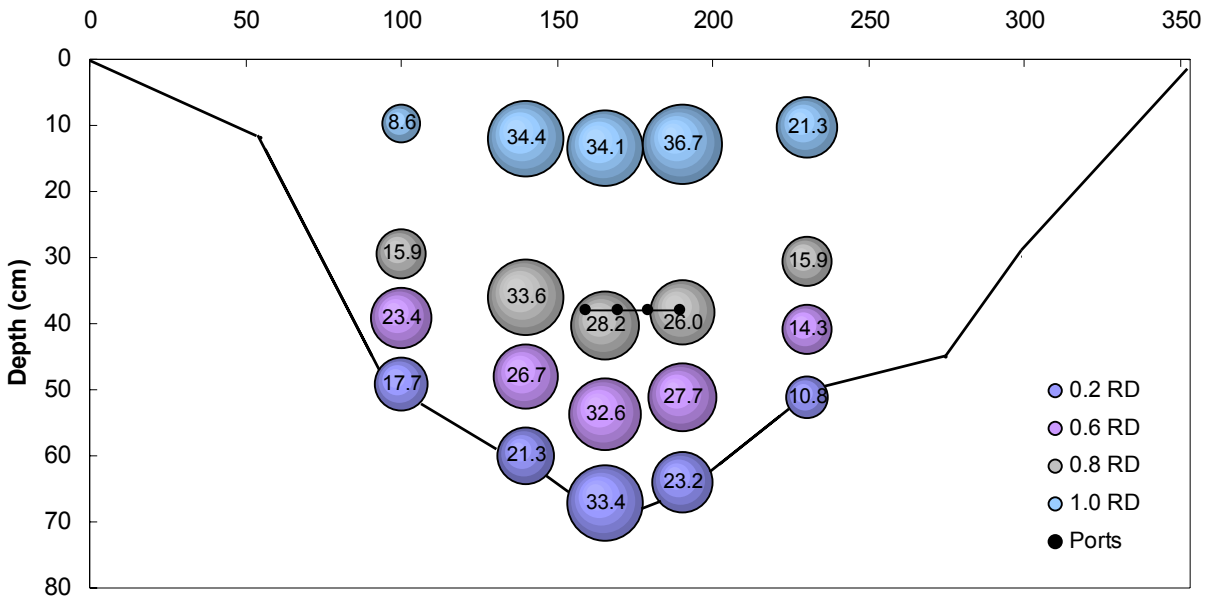

Figure 4-4. Cross-sectional profiling of Sweetwater Branch water velocity, reported in units of cm/s where bubble size is proportional to velocity. Locations of the PSFM intake ports are given by the four black points. The solid black line represents the streambed. This profile was taken on April 24, 2007, and is representative of conditions measured for all steady-state deployments.

Following deployment, sorptive cartridges were returned to the laboratory where the resin and activated carbon portions were carefully removed and prepared for separate extraction procedures. The remaining mass of tracers was extracted from three internal replicates of homogenized activated carbon by 24-hour rotation in 30 mL of isobutyl alcohol (IBA). Extracted tracers were then analyzed using a gas chromatograph with an automated liquid injection (Perkin-Elmer AutoSystem) and flame ionization detector (GC-FID). Sorbed phosphate was extracted from the resin via 24-hour rotation in 30 mL of 2M potassium chloride (KCl). Due to the small amount of resin within each cartridge, no internal replicates were taken. Resin-extracted phosphate samples were then analyzed colorimetrically (Hach DR/4000 Spectrophotometer) using the Hach High Range Total Phosphorus Method 10127 (estimated detection limit 5.0 mg/L PO_4^{3-}). The independent grab samples taken during PSFM deployment were analyzed for phosphate concentration on the same instrument using the Hach Total Phosphorus Method 8190 (estimated detection limit 0.06 mg/L PO_4^{3-}). The tracer and phosphate data were then used to calculate PSFM-derived water and solute fluxes. The fluxes calculated from replicate cartridges of a given deployment were then averaged for comparison to true stream conditions.

4.4 Flux Measurements

During short-term, daytime PSFM deployments, velocity and solute conditions were assumed to be at steady state in Sweetwater Branch. This assumption was based on examination of SJRWMD data that showed significant decreases in both stage and discharge under normal hydrologic conditions only during the overnight hours (Figure 4-5). The overnight period is when discharge from the Main Street WRF to Sweetwater Branch is reduced, which results in some variability of stream conditions. Hence, short-term PSFM deployments that were conducted during daytime hours were expected to avoid this variability and capture only periods

of generally steady-state conditions. Both ethanol and IPA were analyzed for tracer mass remaining over these deployment durations. The tracer masses, along with the resin-sorbed TP masses, generated water and solute fluxes that were compared to true stream fluxes calculated from stream gauging and grab sample analyses.

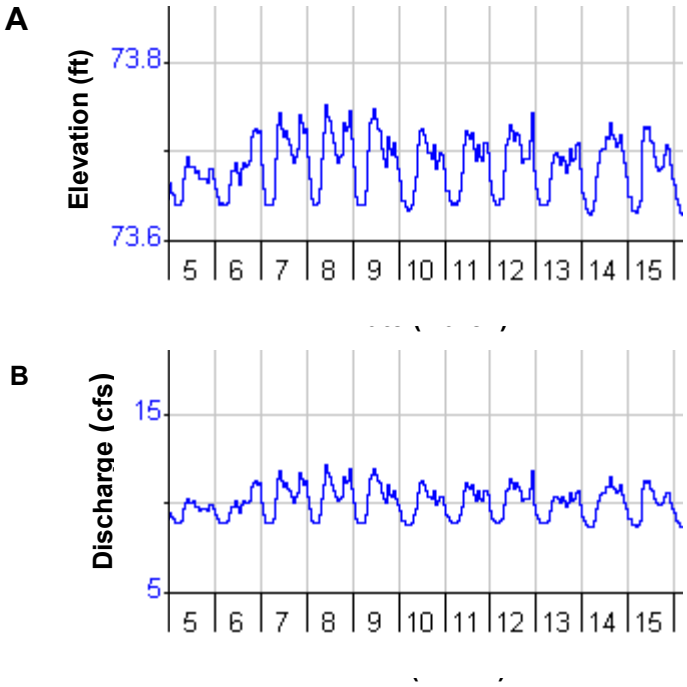

Figure 4-5. Data from SJRWMD monitoring station #01980199, representative of the diurnal cycling of normal hydrologic conditions in Sweetwater Branch. A) Stream stage. B) Stream discharge. (Adapted from SJRWMD, 2007)

4.4.1 Water Fluxes

On average, during short-term deployments in Sweetwater Branch, the PSFM estimated steady-state time-averaged water flux to within 6.6% of true stream conditions. The replicate-averaged experimental water flux data, including percent errors (as compared to true water flux) and statistical p-values for each tracer analyzed during a given deployment, are presented in Table 4-1. The p-values were calculated via two-tailed, paired Student's t-Tests with a threshold of 0.05. The fact that none of the p-values are less than the threshold indicates that there are not significant differences between the true and PSFM-derived water fluxes.

Table 4-1. Comparison of true and PSFM water fluxes during steady-state deployments

Deployment (min)	Tracer	True Water flux (cm/s)	PSFM Water Flux (cm/s)	Percent Error (%)	CV	P-value
40	Ethanol	31.0 ± 2.6	32.5 ± 0.6	4.7	0.02	0.26
40	IPA	31.0 ± 2.6	29.6 ± 2.2	4.6	0.05	0.83
60	Ethanol	24.5 ± 2.2	24.6 ± 1.2	0.5	0.07	0.28
150	IPA	31.0 ± 2.6	28.1 ± 1.2	9.2	0.04	0.11
300	IPA	24.5 ± 2.2	21.1 ± 8	14.1	0.38	0.50
495	IPA	23.0 ± 2.4	23.1 ± 3.8	0.3	0.16	0.98

The comparison between true and PSFM-derived water fluxes are also presented in Figure 4-6. The x-axis error bars represent the error associated with the measurement and interpolation of true water fluxes (velocities). True water velocities were measured during each deployment by hand-held ADV, which internally computes the error associated with each of its measurements. These errors were then subjected to a propagation of error analysis to account for the compounding of uncertainties as velocities were interpolated for each individual port location, and the resulting values were assigned to the x-axis errors bars. The y-axis error bars quantify the variability (standard deviation) of replicate PSFM-derived water flux measurements during a given deployment.

There is a slight trend apparent in the variability of PSFM-derived water fluxes as related to true water velocity. Water fluxes measured at true stream velocities less than 30 cm/s have greater coefficients of variation (CV) than those measured at true velocities greater than 30 cm/s (Table 4-1). This finding might be expected considering that lower velocities do not generate as much flow-inducing head across the sorptive cartridge. However, since the range of velocities offered by Sweetwater Branch was rather limited, it is difficult to make any broad conclusions regarding the variability of PSFM water flux measurements as related to stream velocity.

When considered individually, ethanol and IPA estimated water fluxes to within an average of 2.6 and 9.3%, respectively. While ethanol shows greater accuracy in water flux estimation, its low retardation within the sorptive cartridge does not make it an ideal tracer for longer PSFM deployments. Hence, future investigations should focus on improving the performance and accuracy of IPA as a predictive tracer for long-term PSFM applications.

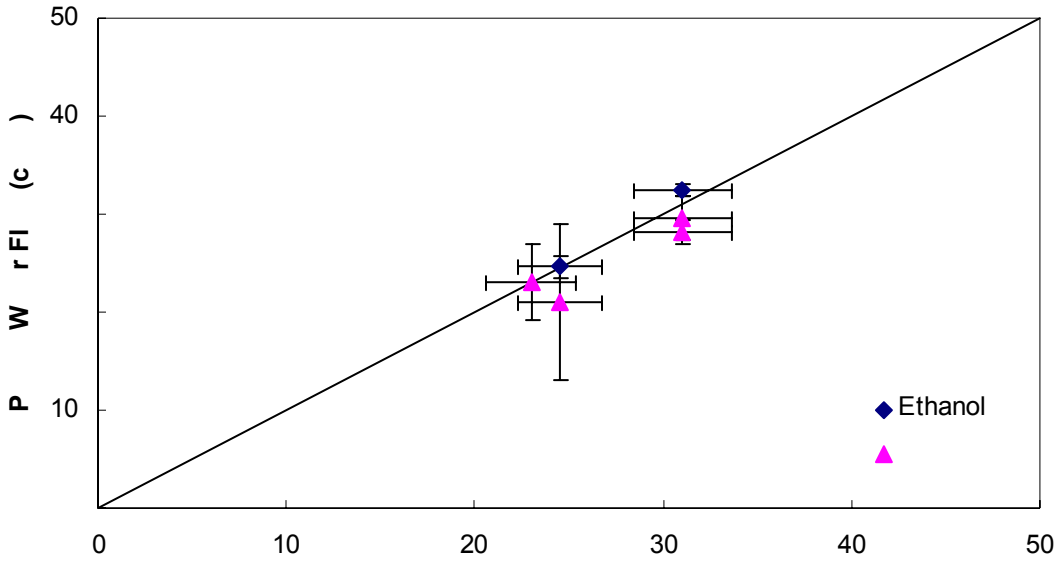

Figure 4-6. Steady-state comparisons of true and PSFM water fluxes. PSFM fluxes were derived from two resident tracers, ethanol and IPA. The solid line represents perfect agreement between true conditions and PSFM estimates.

4.4.2 Solute Mass Fluxes

The PSFM estimated average steady-state phosphate mass fluxes in Sweetwater Branch to within an average of 8.3% of true stream conditions. Table 4-2 presents the replicate-averaged phosphate mass flux data and provides the percent errors of PSFM measurements (as compared to true phosphate flux), as well as statistical p-values for each tracer analyzed during a given deployment. The p-values were again calculated via two-tailed, paired Student's t-Tests with a threshold of 0.05. Similar to the steady-state water flux analysis, none of the p-values are less

than the threshold, and it thus can be concluded that there are not significant differences between the true and PSFM-derived steady-state solute mass fluxes.

Table 4-2. Comparison of true and PSFM-derived steady-state phosphate mass fluxes

Deployment (min)	Tracer	True TP Flux (mg/cm^2min)	PSFM TP Flux (mg/cm^2min)	Percent Error (%)	CV	P-value
40	Ethanol	6.4 ± 0.21	6.1 ± 1.4	5.4	0.23	0.74
40	IPA	6.4 ± 0.21	6.7± 1.9	4.7	0.13	0.82
60	Ethanol	4.4 ± 0.23	3.8 ± 0.5	12.8	0.28	0.09
150	IPA	6.4 ± 0.21	5.8 ± 0.7	10.3	0.13	0.30
300	IPA	4.4 ± 0.23	4.0 ± 1.1	7.6	0.26	0.53
495	IPA	10.5 ± 0.83	9.5 ± 1.5	9.2	0.16	0.24

The comparison between true and PSFM-derived phosphate fluxes is also presented in Figure 4-7, where phosphate data points are given as the product of solute mass flux (*J*) and deployment duration in minutes (*t*). Since solute mass flux is designated by "per time" units, this *Jt* method of presentation allows the results to be considered as a spread of data that relates cumulative phosphate masses to the deployment duration. Error bars for both the x- and y-axes were calculated as the variability (standard deviation) of replicate measurements. Since the calculation of solute mass flux requires a value of stream velocity, the x-axis error bars represent the variability in true *Jt* associated with the slightly differing water velocities at each intake port location. This variability does not include any differences in solute concentration, because all true flux values for a given deployment were calculated using a single stream TP concentration obtained via grab sampling just prior to PSFM deployment. However, the y-axis error bars represent the variability of both tracer-based velocities and resin-sorbed phosphate masses among replicate cartridges of a given deployment.

Although the *Jt* data in Figure 4-7 appears to exhibit a trend of increasing variability with increasing deployment duration, this is an artifact of multiplying the phosphate fluxes by

deployment time, which exaggerates the variability of measurements made over longer periods. When the data are presented as purely phosphate mass flux values, the trend of increasing coefficient of variation with increased deployment duration does not exist (Table 4-2).

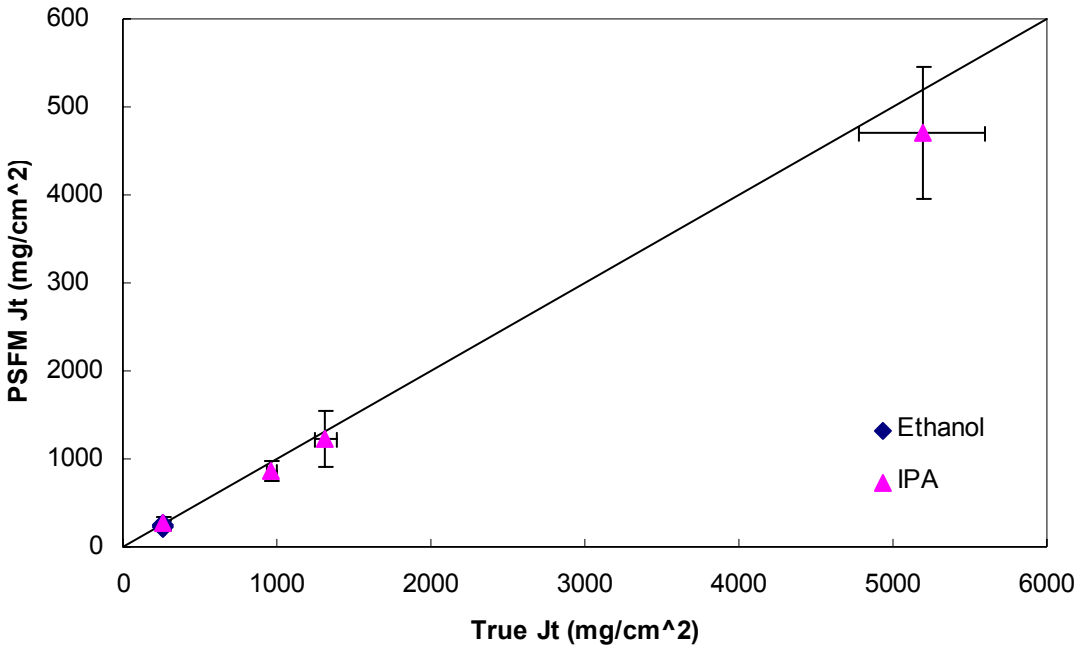

Figure 4-7. Steady-state comparisons of true and PSFM phosphate *Jt*. Values were derived from two resident tracers, ethanol and IPA. The solid line represents the region of perfect agreement between true conditions and PSFM estimates.

When considered separately, ethanol estimated phosphate mass fluxes to within an average of 9.1%, while IPA estimated phosphate mass fluxes to within an average of 7.9%. These accuracies are opposite of those observed for water flux estimation by these two tracers, with IPA being the slightly better predictor of phosphate flux, whereas it was the poorer predictor of water flux. However, when the solute flux measurements made by each tracer are compared with a two-tailed, paired Student's t-Tests (threshold = 0.05), the resulting p-value of 0.33 indicates that there is no significant difference between calculations made using ethanol versus IPA. This indicates that the data is not extensive enough to allow for the definitive determination of which tracer is the most accurate for PSFM data collection.

Given that this study was the very first attempt at field-testing of the PSFM under natural stream conditions, the degree to which the device was able to accurately measure both steady-state water and phosphate mass fluxes in Sweetwater Branch should be considered a success. The ability of the PSFM to estimate fluxes to within less than 10% bodes positively for its continued development and future use in a variety of water resources research and management applications.

4.5 Constant Relative Depth Deployment Apparatus Performance

In addition to verifying the accuracy of PSFM flux measurements, field experiments were also used as a venue for demonstrating the function of the CRD deployment apparatus. While steady-state deployments did not offer an opportunity to evaluate the effectiveness of the apparatus for maintaining instrumentation at six-tenths relative depth as stream stage varied, the relatively static conditions did provide circumstances under which the first-order operation of the CRD apparatus (to position the PSFM at six-tenths depth) could be assessed and improved.

Early in the apparatus design process, it became apparent that merely attaching the PSFM cylinder at six-tenths the length of the float arm would not position the intake port of the PSFM at six-tenths relative depth, due to location of the intake ports at vertical position above the point of attachment. Instead, placing the intake ports at the desired six-tenths of the total water depth required an offset calculation for positioning attachment of the PSFM cylinder further down the length of the CRD float arm. The calculation for the offset distance was derived based on the angle between the float arm and streambed at a given water depth and the size and port positioning of the PSFM, and is given by

$$L_o = \frac{0.6 D_c L_{fa}}{d} \tag{4-1}$$

where L_o [L] is the required offset distance as measured down from the point of six-tenths of float arm length, D_c [L] is the diameter of the PSFM cylinder and bead-bearing system, d [L] is the total water depth, and L_{fa} [L] is the length of the CRD float arm. The factor of 0.6 is included in the equation to account for the specific PSFM design used in this study, where the intake ports are positioning at 60% the height of the diameter. If a given PSFM design had intake ports located at a different position relative to the cylinder diameter, this factor could be adjusted accordingly.

Figure 4-8 demonstrates the effects of variations in PSFM diameter and total water depth on the required offset distance. For a fixed water depth, the offset distance increases with PSFM diameter to account for the greater disparity between the attachment point and in the intake port location. In contrast, as the PSFM cylinder become sufficiently small, the distance between its attachment to the float arm and the location of the intake ports becomes negligible and no offset is required. For a fixed diameter, the required offset of the PSFM decreases as water depth increases until the float arm is perfectly vertical (float arm length equals total water depth). At this position, the offset needs to be only as large as the distance between the attachment point and the intake ports.

The dependence of the offset distance on water depth becomes problematic when considering performance of the CRD apparatus under conditions of varying stream stage. During transient deployments in which water level is rising and falling, it is not possible or practical to adjust the offset according to these fluctuations, and the rotation of the PSFM to maintain is position normal to water flow inhibits the accuracy of the CRD apparatus. Setting the offset according to only initial water depth creates positioning errors during flux data collection, because with rotation of the cylinder as stream stage varies, the position of the intake ports

relative to the attachment point on the float arm changes, and the offset to which the apparatus was initially set becomes incorrect for maintaining the intake ports at the desired six-tenths relative depth. The error associated with this inaccuracy can be calculated by

$$PE_{L_o} = \frac{d_R - \frac{\left(d_R L_{fa}\right) + L_o - \left(\frac{0.6 L_{fa} D_c}{d}\right)}{L_{fa}}}{d_R} * 100 \qquad (4\text{-}2)$$

where PE_{Lo} [%] is the deployment depth percent error associated with the offset distance and d_R [-] is the desired relative depth of deployment. Again, the factor of 0.6 corresponds to the specific intake port positioning of the PSFM designed for this study (60% of the height of PSFM diameter), which could be adjusted use with for other device designs. Figure 4-9 demonstrates that these potential errors are minimized as PSFM diameter decreases, because less original offset distance is required. The trends also suggest that when deploying the PSFM via CRD apparatus under conditions of fluctuating water level, the offset should be set according to the lowest expected water level, as the errors incurred with water level increases are less severe as compared to those associated with water level decreases.

While the effects of varying water depth on PSFM positioning did not need immediate consideration during steady-state deployments, correct positioning was still not guaranteed even when stream stage was constant. Successive deployments exhibited intake ports depths that were not at six-tenths, but instead at 0.5, 0.55, 0.58, and 0.56 of the total water depth. There were several observed problems that contributed to these inaccuracies in the field. Some of these problems occurred only for the first field deployment, during which superficial design flaws in the CRD apparatus were initially identified. For instance, the original floats chosen for use in the CRD design did not have sufficient buoyancy or surface area to support the PSFM and properly

position the top of the float arm at the water surface. This resulted in drawdown of the entire apparatus and incorrect positioning of the PSFM intake ports. However, the substitution of higher-surface area floats corrected this problem for subsequent deployments.

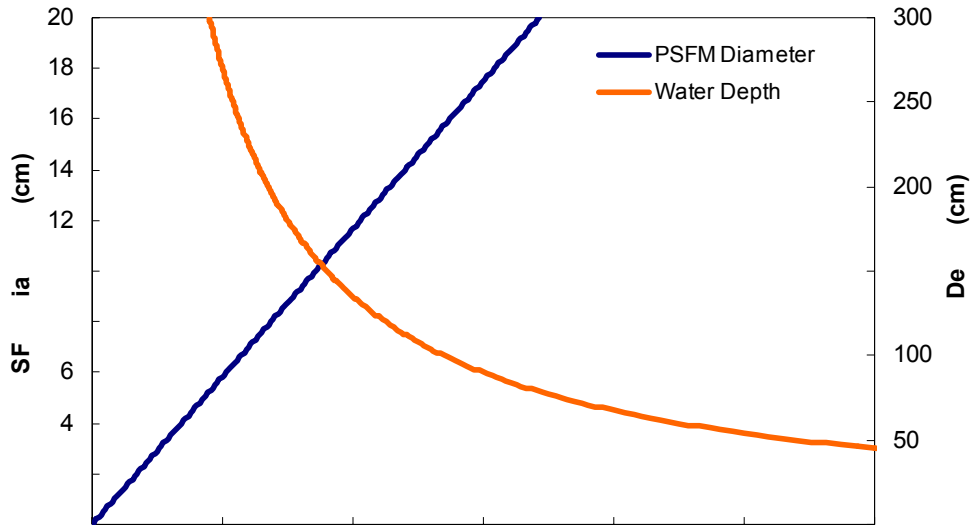

Figure 4-8. CRD offsets required for various PSFM diameters and water depths. Offsets due to variations in diameter are calculated for a fixed water depth (70 cm), and offsets due to variations in water depth are calculated for a fixed diameter (15 cm).

Another factor that contributed to the inaccuracy of positioning was the presence of a slight downward slope in the streambed at the PSFM deployment site. To precisely position the PSFM, the geometry of the CRD design requires that the streambed be parallel to the water surface over the length of the apparatus. If this is not the case and a local perturbation is streambed slope is present, then the PSFM will be vertically positioned at six-tenths of the total water depth measured at the base-end of the float arm, which will not correspond to six-tenths of the total depth where the PSFM is actually located slightly downstream (Figure 4-10). In the case of a downward streambed slope, the PSFM will be located at less than six-tenths depth, and in the case of an upward slope the PSFM will be located at more than six-tenths relative depth. The error associated with these positioning inaccuracies can be calculated by

$$PE_{slope} = \frac{\tan\gamma\left(L_{fa}\left(1-d_R\right)\right)\cos\left(\sin^{-1}\left(\frac{d_{CRD}}{L_{fa}}\right)\right)}{d_{CRD}+\left[\tan\gamma\left(L_{fa}\left(1-d_R\right)\right)\cos\left(\sin^{-1}\left(\frac{d_{CRD}}{L_{fa}}\right)\right)\right]} * 100 \quad (4\text{-}3)$$

where PE_{slope} [%] is the deployment depth percent error as a result of sloping streambed, d_{CRD} [L] is the water depth at the base of the CRD apparatus, and γ [degrees] is the slope angle of the streambed. Deployment depth error increases with increasing slope angle as the difference between d_{CRD} and d_{PSFM} ([L], water depth at PSFM) becomes greater, and decreases with increasing water depth as the float arm approaches vertical (Figure 4-11). If there is prior knowledge of streambed elevations at a given deployment site, there is potential to correct for known slopes in the CRD design. However, in streams such as Sweetwater Branch that have very sandy beds with constantly changing morphology, this is not always possible.

Despite the complexities and limitations of deploying the PSFM with the CRD apparatus encountered in this study, the CRD still has potential utility as a hydrologic monitoring tool. While the apparatus did not prove to be best suited for general use with the PSFM, which has specific requirements to maintain its vertical, unobstructed position within the stream flow field, the CRD is still likely to work well for other monitoring applications in which the measurement device can be exactly positioned at the point of six-tenths the length of the float arm. Such potential applications include the long-term placement of autosampler inlet ports, water quality sensors, and velocity meters at specified relative depths. Hence, with continued development and testing, the CRD apparatus should prove itself to be a valuable addition to the variety of equipment and technologies available for water resources research and management.

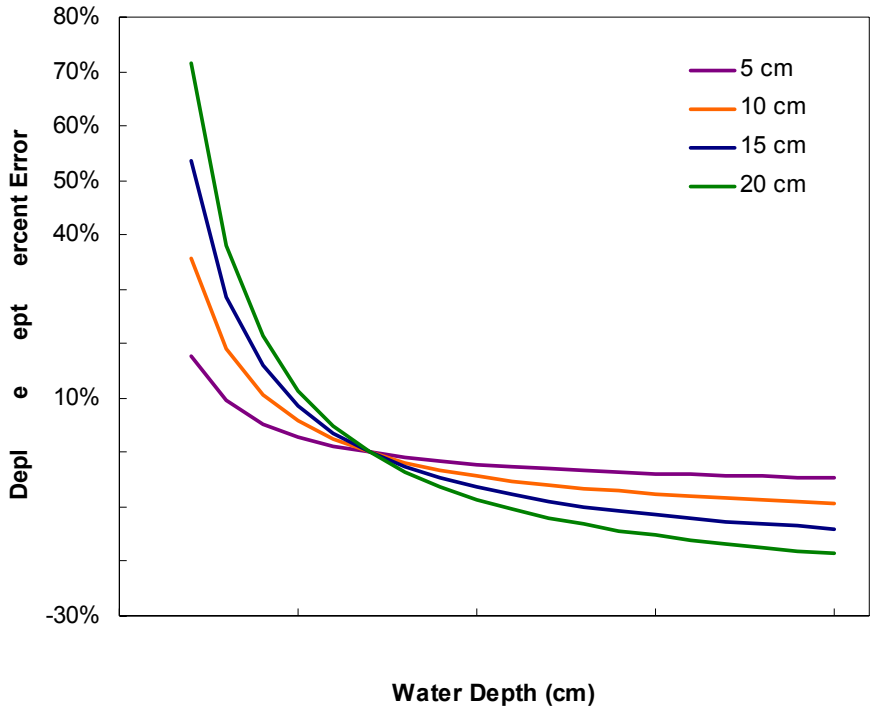

Figure 4-9. Error in the six-tenths relative depth positioning of the PSFM as water level fluctuates. The four lines represent PSFMs of varying diameters (5, 10, 15, and 20 cm). The offset for each diameter was set for a CDR arm length of 200 cm and water depth of 70 cm. Positive errors indicate that the PSFM intake ports are located at a relative depth less than six-tenths, while negative errors indicate the ports are at a relative depth greater than six-tenths.

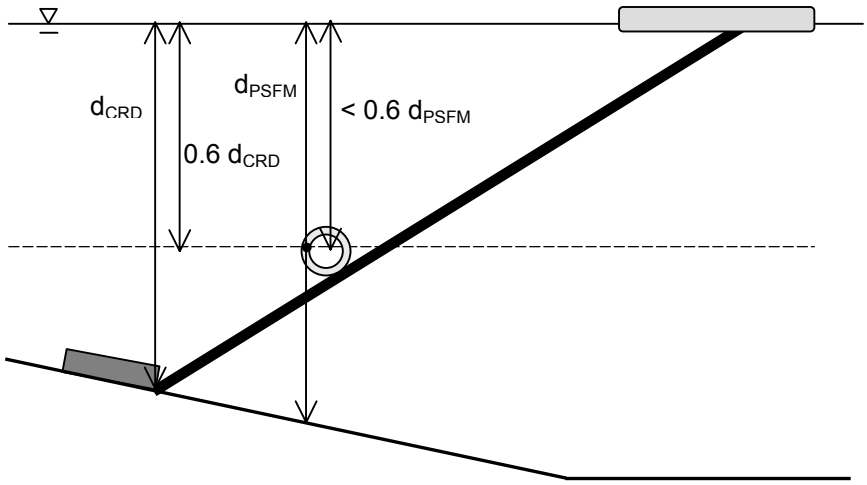

Figure 4-10. Effect of streambed slope on CRD positioning of the PSFM. When the bed slopes downward, the PSFM is located in a greater depth of water than the fixed end of the float arm and it is no longer located at six-tenths relative depth.

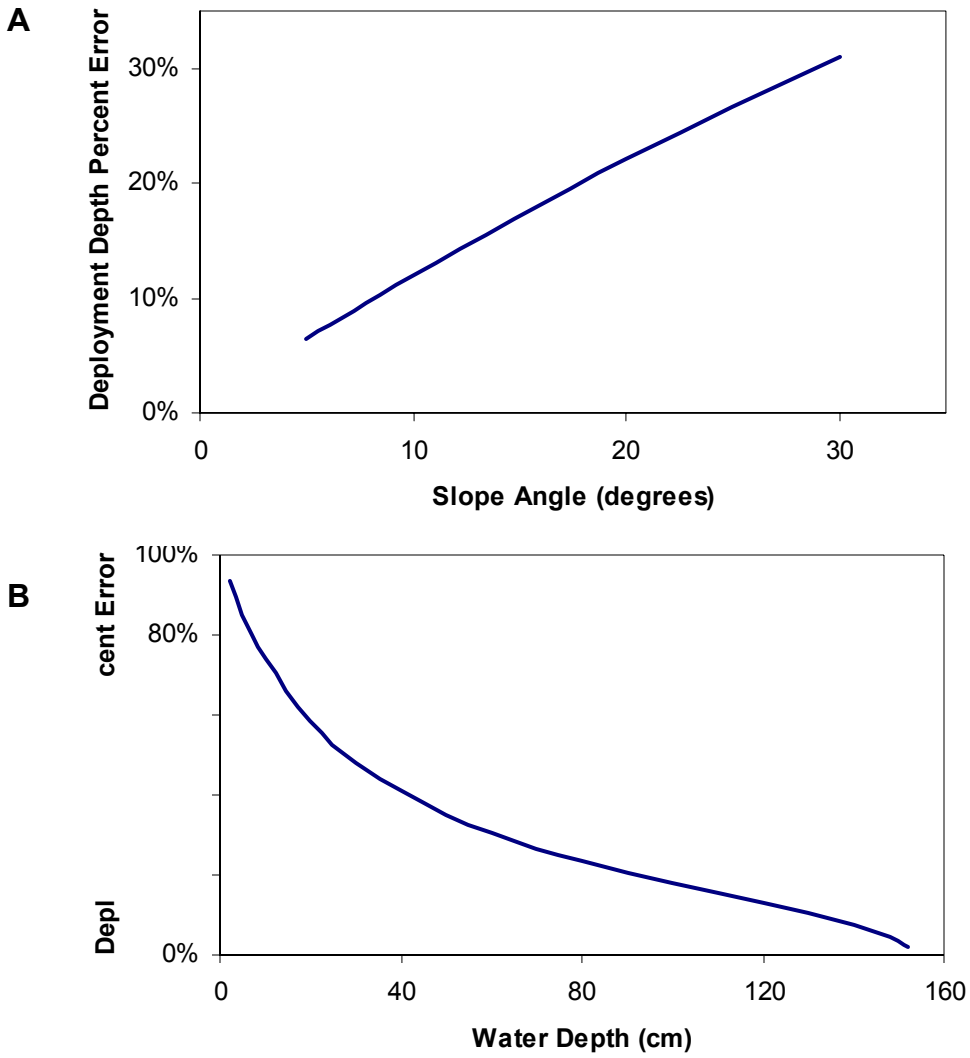

Figure 4-11. Errors in relative depth positioning of PSFM intake ports associated with sloping streambed. A) Effects of increasing slope angle at a constant water depth, d_{CRD} = 70 cm. B) Effects of increasing water depth at a constant streambed slope angle of 25°.

CHAPTER 5
TRANSIENT FIELD DEPLOYMENT

5.1 Introduction

Given that the natural environment is rarely at steady state, once the fundamental performance and accuracy of the PSFM has been verified, field-testing under transient conditions is necessary to demonstrate its broader scale applications. However, there are theoretical limitations to applying the PSFM technology to fluctuating environmental conditions. While the PSFM may perform adequately under circumstances of certain transient characteristics, its cumulative, time-averaged results do not provide information concerning the timing or intensity of varying water and solute fluxes. Further, the quadratic nature of PSFM velocity measurements may lead to inaccurate assessments of true stream conditions.

This study examined performance of the PSFM under conditions of limited diurnal variability and also considered performance implications during the more pronounced transience of hypothetical storm events. Preliminary results showed that the PSFM was reasonably effective under conditions of limited variability, but the device design was not able to withstand the force of a storm event within Sweetwater Branch. Hence, complete transient development and testing remains for future work.

5.2 Passive Surface Water Flux Meter Limitations

The PSFM generates water and solute fluxes that represent the time-averaged conditions within a flowing surface water body over the deployment duration. This implies that data derived from the device does not indicate the timing or degree of fluctuating conditions, which can inhibit appropriate interpretation of the data. Klammler et al. (2007) described the restricted conditions under which the PSFM theory may be appropriately applied to transient surface waters. These conditions include limited variations in flow velocity and solute concentration, or

the absence of correlation between flow velocity and solute concentration. However, during more dynamic or correlated events, PSFM-derived cumulative fluxes are likely to misrepresent true conditions as compared to more traditional time-series integration methods of flux determination.

To demonstrate the differences in solute loads calculated from PSFM measurement and time-series integration, continuous records of velocity and concentration from three hypothetical transient scenarios are shown in Figure 5-1. The three scenarios have the same average water velocities (37.8 cm/s) and solute concentrations (1.75 mg/L), but differ in the timing and intensity of the solute concentration fluctuations. Scenario A depicts a pulse in water velocity that is accompanied by a simultaneous pulse in nutrient concentration. Scenario B portrays a water velocity pulse followed by a delayed solute concentration pulse, and Scenario C shows a water velocity pulse accompanied by a less intense, but more prolonged concentration pulse. The time-series fluxes are calculated by integrating the incremental flux for each time step (30 minutes) over the deployment duration (24 hours). PSFM fluxes are calculated as the product of the time-averaged velocity and flux-averaged concentration.

Even though the three scenarios have the same time-averaged parameters, they each generate different solute fluxes via PSFM-based calculations over the 24-hour period: 5.61, 3.01, and 4.31 mg/cm^2/s for Scenarios A, B, and C, respectively. This occurs because higher solute concentrations corresponding to periods of higher stream velocity result in more solute mass entering and being retained within the sorptive cartridge. The time-series fluxes also vary among the scenarios, because flux calculations incorporate the multiplied effects of velocity and concentration, hence higher fluxes occur during periods when water velocity and solute concentration are both experiencing increases. (Figure 5-2). With a time-series flux of 3.03

mg/cm^2/s, Scenario B shows only 0.52% difference between the PSFM and integrative calculations, however this is to be expected given the relatively uncorrelated timing of the fluctuations (R^2=0.2262). The integrative fluxes for Scenarios A and C, 4.14 and 3.57 mg/cm^2/s, respectively, are more dissimilar from those produced by the PSFM-based calculations, with percent differences of 30.3 and 18.8%, respectively. These discrepancies occur because both these scenarios exhibit concurrent (correlated) increases in water velocity and solute concentration, a common observation in natural surface water systems that results from solute flushing of the watershed due to storm water runoff (Li et al., 2007; Taebi and Droste, 2004; Lee et al., 2002; Bertrand-Krajewski et al., 1998; Deletic, 1998). Given that flow variability within the sorptive cartridge is not directly proportional to flow variability within the stream under transient velocity conditions, the quadratic mean of stream velocity as reported by the PSFM can misrepresent the actual stream velocity. In effect, the true conditions of transient fluxes can be obscured by the quadratic nature of the PSFM measurements.

5.3 Transient Deployment Tests

Despite the known limitations of the PSFM for transient flux measurement, this study attempted to investigate actual field performance of the device under naturally variable stream conditions. Two transient deployment tests were conducted; one to characterize conditions of limited variability over a diurnal cycle and the other to capture the drastic fluctuations of a storm event. Both tests utilized the same deployment site and methods as the preceding steady-state experiments, with the addition of several instruments for continuous monitoring of stream conditions over the 24-hour deployment durations. A SonTek Argonaut ADV measured water velocity every 30 minutes, an In-Situ Level Troll 500 transducer measured water depth every 15 minutes, and an ISCO 3700 Sampler collected water samples every 60 minutes for subsequent laboratory TP analysis. The continuous time-series of velocity and concentration data were

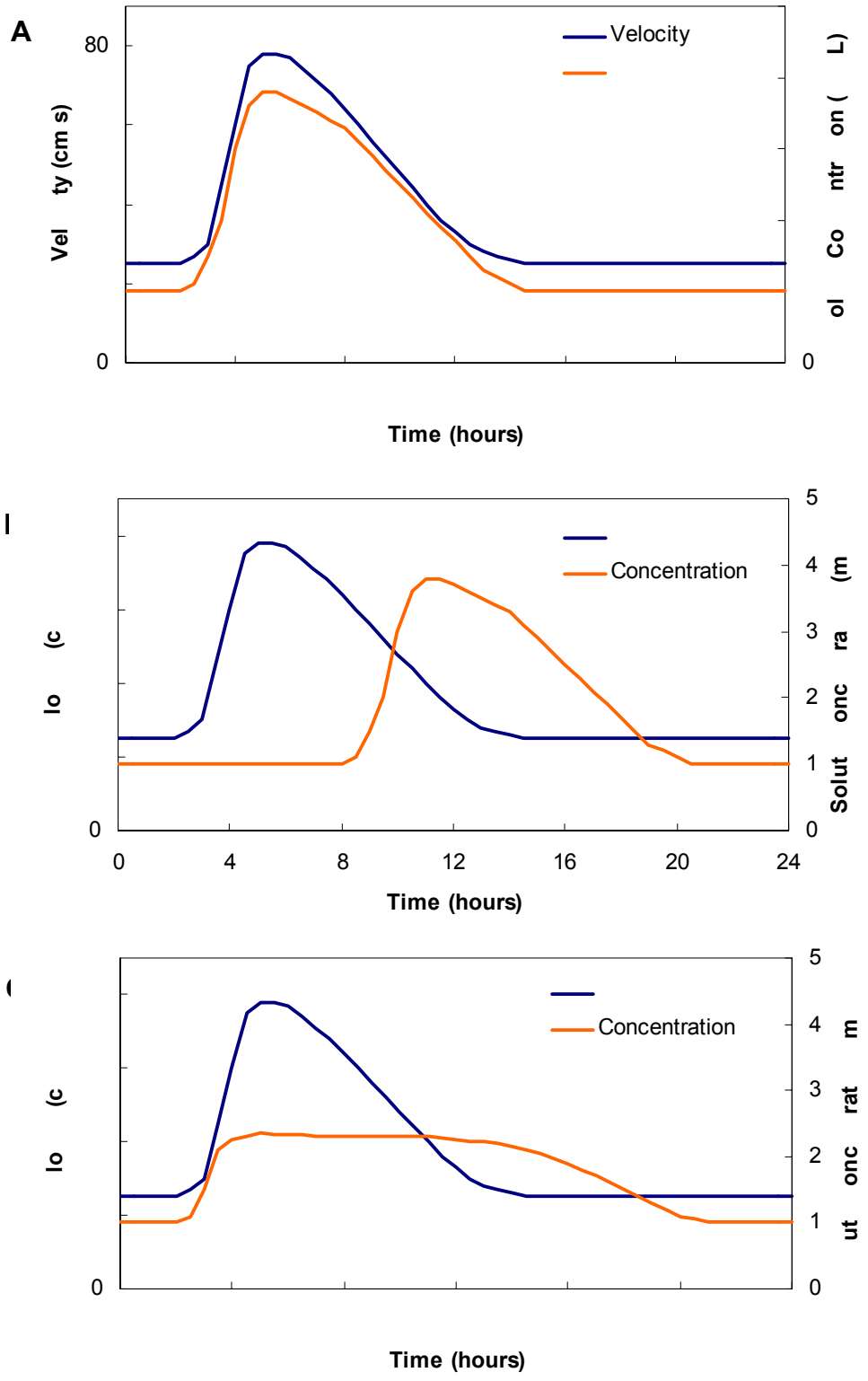

Figure 5-1. Three scenarios for assessing PSFM versus time-series integration estimates of solute loading. The scenarios have identical time-averaged water velocity and solute concentration. A) Scenario A. B) Scenario B. C) Scenario C.

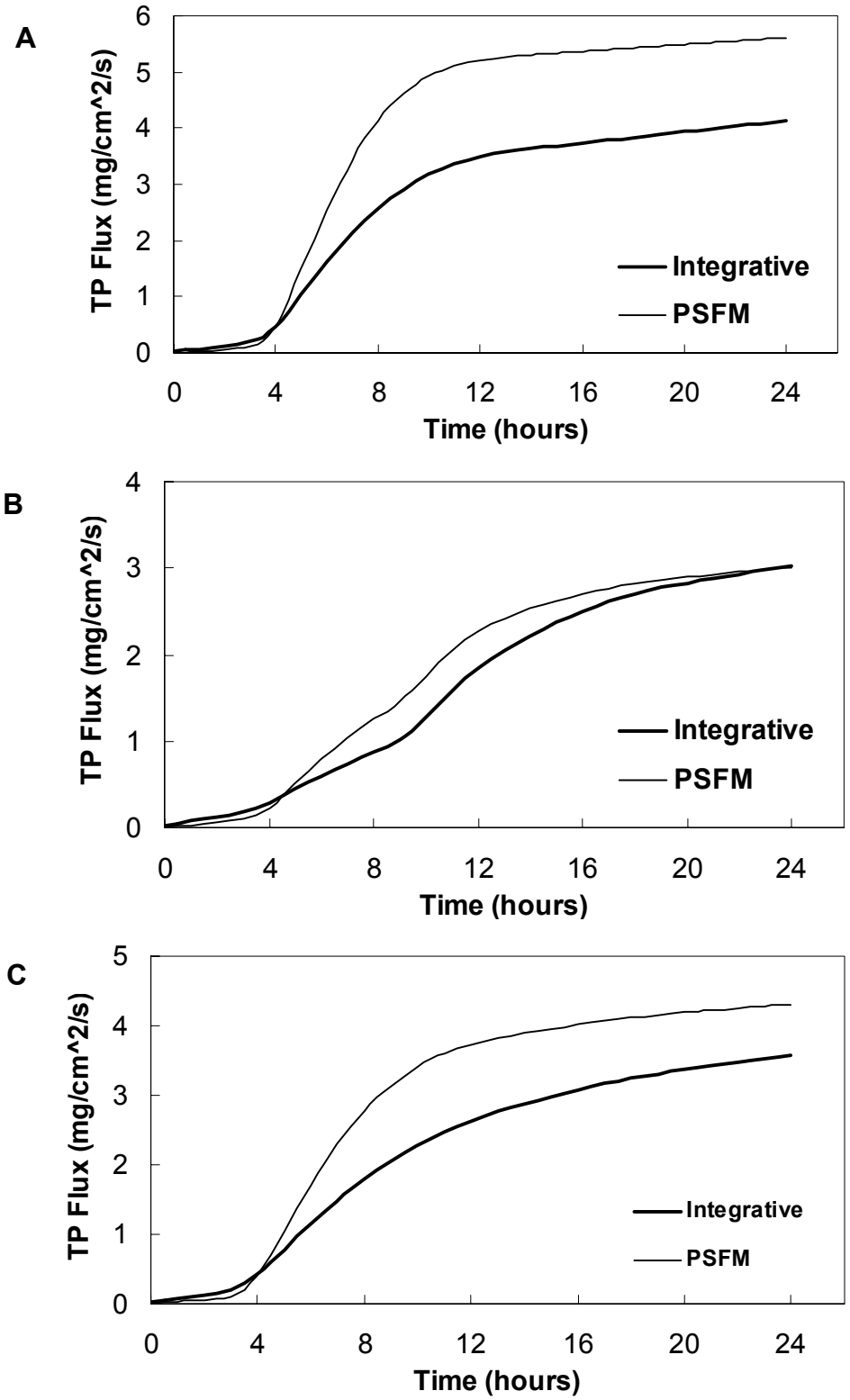

Figure 5-2. Hypothetical TP fluxes generated from PSFM and time-series integration methods. The PSFM best estimates the true cumulative flux of Scenario B, while over predicting fluxes of Scenarios A and C. A) ScenarioA. B) Scenario B. C) Scenario C.

used to calculate the true cumulative water and phosphate fluxes for comparison to PSFM-derived estimates. The water depth data were used to determine stream cross-sectional area for both PSFM and integrative load estimates.

5.3.1 Diurnal Deployment

Sweetwater Branch was considered an appropriate location for initial transient field-testing, because of the diurnal wastewater inputs associated with municipal water usage. Continuous monitoring of normal (non-storm event) flow conditions over the 24-hour deployment period indicated fluctuating trends of limited variability in water velocity, water depth, and TP concentration (Figure 5-3). Both velocity and depth experienced decreases during the overnight hours from approximately 10:30PM to 9:30AM, while TP exhibited a slight increase during the same period. The velocity and depth trends were expected, given the decreased volume of discharge to the creek by the GRU Main Street WRF during the evening, when there is less municipal consumption and therefore less wastewater requiring treatment. However, if the wastewater discharge was the main source of TP to the creek, such flow reductions would also lead to decreased phosphate levels. The observed increase in TP suggests that the WRF may not actually be the primary TP source, and that other sources, such as septic tank leakage or phosphoric minerals, are contributing comparable amounts of phosphorus to the system.

PSFM deployment results over the diurnal period demonstrated relatively good comparison to true fluxes and loads, as derived from integration of the continuous velocity and TP concentration profiles (Table 5-1). Due to the extended deployment duration, IPA and TBA (the tracers with the highest retardation within the sorptive cartridge) were analyzed for tracer mass remaining to be used in PSFM calculations. Calculations made using IPA estimated water flux, TP flux, and TP load to within 13.5, 5.6, and 5.6%, respectively, and calculations made

using TBA estimated the same parameters to within 4.9, 22.1, and 22.1%, respectively. It is not immediately conclusive which tracer performed better for flux determination over the 24 hours, because p-values indicate that the IPA-estimated water flux is significantly different from the true value, while the TBA-estimated TP flux is significantly different from the true value.

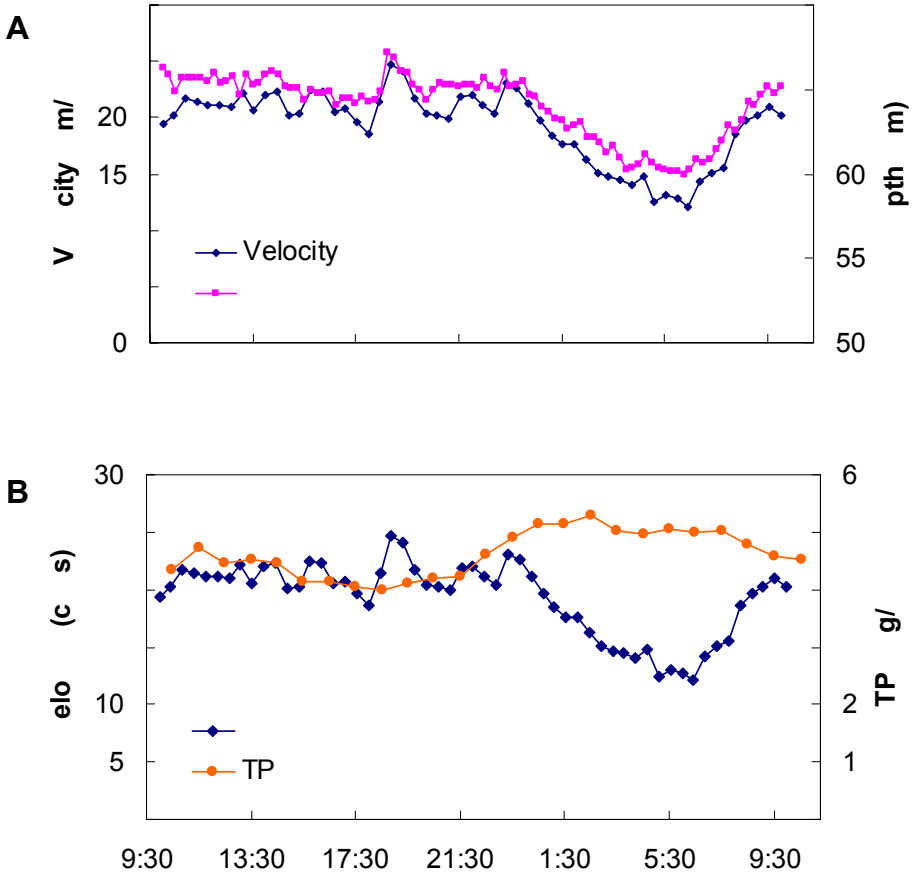

Figure 5-3. Trends recorded in Sweetwater Branch during the diurnal deployment under normal flow conditions. A) Comparison of water velocity and depth, which are correlated with in R^2 value of 0.9517. B) Comparison of water velocity and TP concentration.

It is likely that these results were reasonably accurate because the degree of velocity and concentration transience falls into the range of limited variability qualitatively described by Klammler et al. (2007) as appropriate for PSFM flux determination. Primarily, the variations in water velocity were small enough that the arithmetic mean could be approximated well by the measured quadratic mean, and the variations in phosphate concentration were not significant.

Hence, the observed variation of these parameters did not drastically affect flux estimates derived from the PSFM theory. This assumption is confirmed by the comparison of ideal PSFM behavior under the observed conditions to the integrative estimates (similar to the transient scenario comparisons performed above). Had tracer performance been optimal, allowing the PSFM to perfectly measure water velocity and solute concentration as compared to the true integrative estimates, the percent difference between PSFM and time-series integration estimates of TP flux and load would have been only 1.0 and 0.5%, respectively. Therefore, the diurnal variability in Sweetwater Branch was not drastic enough to deviate from the PSFM theory applied to steady-state conditions and was able to provide reasonable approximations of the transient water and solute mass fluxes.

Table 5-1. Comparison of true and PSFM fluxes and loads during diurnal transient deployment

Tracer/Parameter	True Value	PSFM Value	Percent Error	CV	P-value
IPA					
Water Flux (cm/s)	20.8 ± 2.3	18.0 ± 1.3	13.5	0.07	0.02
TP Flux (mg/cm^{2}min)	5.8 ± 0.4	5.4 ± 0.6	5.6	0.11	0.33
TP Load (kg/day)	94.1 ± 5.9	88.7 ± 10.0	5.6	0.11	0.33
TBA					
Water Flux (cm/s)	20.8 ± 2.3	21.8 ± 2.2	4.9	0.10	0.28
TP Flux (mg/cm^{2}min)	5.8 ± 0.4	4.5 ± 0.4	22.1	0.10	0.02
TP Load (kg/day)	94.1 ± 5.9	73.2 ± 7.1	22.1	0.10	0.02

5.3.2 Storm Deployment

The PSFM was also deployed during a storm event to assess performance of the device under conditions of more pronounced velocity and solute concentration variability. However, the effects of a moderate rainstorm (0.2 cm rainfall over one hour) overwhelmed the physical capabilities of the PSFM designed for this study. Due to its small channel, large impervious area in the watershed, lack of stormwater retention, and relatively high relief (RPG, 2003), Sweetwater Branch responded rapidly to the rainfall, resulting in a violent storm surge that rushed through the creek. The force of the surge displaced and obstructed the PSFM, CRD

apparatus, and independent monitoring equipment such that only incomplete data for the deployment were recovered.

Prior to being washed downstream, the installed transducer indicated that water depth increased from 77 to 135 cm in the 105 minutes from the beginning of rainfall to the onset of the storm surge (Figure 5-4), and personal observation indicated that the pre-rainfall water velocity of approximately 28 cm/s had increased by an order of magnitude. Three sets of manual grab samples (with three replicates each) collected before, during, and after the storm surge indicated that TP concentration fluctuated from 7.6 to 11.0 and back to 7.2 mg/L over the course of the event. Before and after measurements indicated that the storm surge also deposited approximately 40 cm of sand in the location where the PSFM and CRD apparatus had been originally deployed. So while independent measurements observations indicated that Sweetwater Branch was in fact experiencing highly transient conditions, the PSFM was unfortunately unable to capture this dramatic event.

5.4 Future Transient Testing and Development

There is an obvious need for more complete transient PSFM field-testing to investigate both tracer performance over long deployment durations and accuracy of the device during more markedly variable conditions. Given the theoretical limitations of the PSFM model, it is likely that its transient flux determination will not provide reasonable estimates of true stream behavior under a variety of variable conditions. Hence, this will require the development of additional theory for the application of PSFM technology to transient surface water systems. There are also design modifications necessary for future deployments during storm events. Future PSFM designs must be more robustly constructed and better anchored to the streambed in order to withstand potentially brutal storm surge condition.

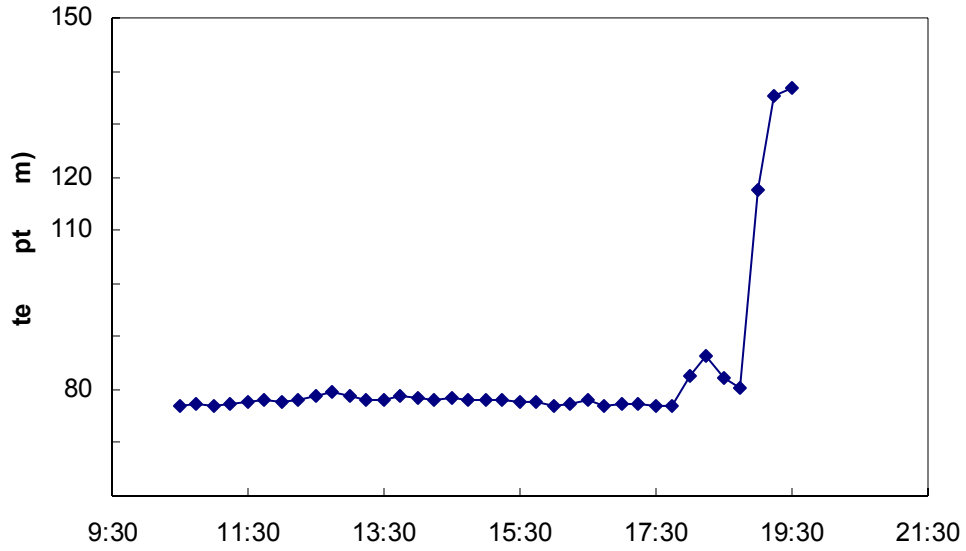

Figure 5-4. Water depth in Sweetwater Branch before and during the storm event. Rainfall began at approximately 17:45, and data collection was interrupted when the transducer was displaced by the storm surge at 19:30.

CHAPTER 6
CONCLUSIONS AND FUTURE WORK

The purpose of this research was to further the development of the Passive Surface Water Flux Meter and demonstrate its accurate measurement of water and solute mass fluxes in natural stream channels. Given the previous successes of the PSFM in laboratory settings, this continued development and transition to field-scale monitoring involved characterizing tracer behavior within the sorptive cartridge, adapting the device design for use in natural streams, and testing the device under both steady-state and transient stream conditions. The use of the CRD apparatus was also incorporated into deployment of the PSFM to demonstrate its usefulness for continuous positioning of monitoring equipment at the depth of average stream velocity.

The tracer characterization portion of the study involved both a series of laboratory elution tests and modeling of the elution data in HYDRUS-1D. Retardation factors for each of the four tracers used in flux determination calculations (methanol, ethanol, IPA, and TBA) were derived from the elution curves via the linearization method (Hatfield et al., 2004). The elution curves combined with extractions of the tracer mass remaining on the porous media confirmed mass balance of the tracers. Modeling of the tracer desorption reactions demonstrated that while methanol and ethanol experienced equilibrium desorption within the PSFM cartridge, IPA and TBA experienced rate-limited desorption. The departure from equilibrium behavior increased with tracer retardation, indicating that more reactive tracers experience increased rate-limitation within the cartridge. The degree of rate limitation also increased with flow velocity, which is most likely the result of slow tracer diffusion. These findings have implications for the use of IPA and TBA for accurate flux determination, specifically at high stream velocities and long deployment durations. Hence, the hypothesis that resident tracers are experiencing equilibrium desorption within the PSFM cartridge was only partially confirmed.

Field-testing of the PSFM was conducted at a site within Sweetwater Branch, an urbanized creek in Gainesville, Florida. The site received steady, predictable stream flows and phosphate concentrations under normal conditions, but was also highly susceptible to the effects of storm events, making it an ideal choice for both steady state and transient testing. The cylindrical device designed for this study was found to perform well under natural steady-state flow conditions, accurately measuring water and phosphate mass fluxes to within 10%. The device was also shown to be preliminarily effective under transient conditions of limited variability, measuring water and phosphate mass fluxes to within 22%. However, hypothetical simulations of more pronounced transient conditions demonstrated that the quadratic-mean character of PSFM measurements can lead to inaccurate flux estimations. These findings confirm the hypothesis of accurate PSFM flux measurement under steady-state conditions, though complete investigation of its abilities and accuracy under transient conditions remains for future work.

PSFM field tests were also used as an opportunity to demonstrate the function of the CRD apparatus, a novel technology for the deployment of monitoring equipment at constant relative depth. For this study, the CRD was used to deploy the PSFM at six-tenths relative depth, the location of average stream velocity. The CRD apparatus proved to be relatively successful in its intended function, but several limitations were identified over the course of the deployments. These limitations include the design modifications necessary to accommodate the offset distance required to position the PSFM intake ports at the proper relative depth and compromised performance when deploying the apparatus in a region with local perturbations in streambed slope. So while the hypothesis of continuous positioning at six-tenths relative depth is generally supported, given the specific spatial requirements of the PFSM device, the apparatus is not best

suited for deploying the current PSFM design. However, the CRD deployment apparatus should not be discounted for use in other water resources monitoring applications.

Continued development of the PSFM requires additional work on various aspects of the device. There is a need for further research to determine the most appropriate and accurate tracers for PSFM flux determination. This could include either modifications to the PSFM theory to account for rate-limited tracer behavior, or the investigation of alternate organic tracers that will experience predictable equilibrium behavior over long deployment durations. There is also a need to perform additional steady state field-testing over a wider range of stream velocities and solute concentrations, and complete transient field-testing over a broad range of variable flux conditions, including storm events. This will help to provide more comprehensive verification of the PSFM for accurate flux measurement.

Future directions for field-testing also include deployment of a more hydrodynamic-hydrofoil PSFM, and extending analyses to different solutes of interest, such as nitrates, heavy metals, or emerging contaminants. Determination of better methods for the hydrologic characterization of "true" stream conditions would be advantageous for more accurate comparison to PSFM measurements, and investigations should also establish appropriate methods for interpolating PSFM point measurements to accurately characterize the flux and loading behavior of entire flowing surface water bodies.

Despite the needs for further research and development, the PSFM has made progress toward being marketed for widespread academic and commercial use. During this study, the PSFM successfully demonstrated its potential as a low-cost, low-maintenance tool for a variety of water resources research and management activities, such as watershed quality monitoring and TMDL development.

LIST OF REFERENCES

Alvarez, D.A., Stackelberg, P.E., Petty, J.D., Huckins, J.N., Furlong, E.T., Zaugg, S.D. and Meyer, M.T., 2005. Comparison of a novel passive sampler to standard water-column sampling for organic contaminants associated with wastewater effluents entering a New Jersey stream. Chemosphere, 61(5): 610-622.

Annable, M.D., Hatfield, K., Cho, J., Klammler, H., Parker, B.L., Cherry, J.A. and Rao, P.S.C., 2005. Field-scale evaluation of the passive flux meter for simultaneous measurement of groundwater and contaminant fluxes. Environmental Science & Technology, 39(18): 7194-7201.

Aulenbach, B.T. and Hoopert, R.P., 2006. The composite method: an improved method for stream-water solute load estimation. Hydrological Processes, 20(14): 3029-3047.

Bertrand-Krajewski, J.L., Chebbo, G. and Saget, A., 1998. Distribution of pollutant mass vs volume in stormwater discharges and the first flush phenomenon. Water Research, 32(8): 2341-2356.

BOR, 2001. Water Measurement Manual: A guide to effective water measurement practices for better water management, Bureau of Reclamation, U.S. Department of the Interior. U.S. Government Printing Office, Washington, D.C. http://www.usbr.gov/pmts/hydraulics_lab/pubs/wmm/.

Branco, B., Torgersen, T., Bean, J.R., Grenier, G. and Arbige, D., 2005. A new water column profiler for shallow aquatic systems. Limnology and Oceanography-Methods, 3: 190-202.

Brusseau, M.L., 1992. Nonequilibrium Transport of Organic-Chemicals - the Impact of Pore-Water Velocity. Journal of Contaminant Hydrology, 9(4): 353-368.

Brusseau, M.L., Larsen, T. and Christensen, T.H., 1991. Rate-Limited Sorption and Nonequilibrium Transport of Organic-Chemicals in Low Organic-Carbon Aquifer Materials. Water Resources Research, 27(6): 1137-1145.

Burke, P.M., Hill, S., Iricanin, N., Douglas, C., Essex, P. and Tharin, D., 2002. Evaluation of preservation methods for nutrient species collected by automatic samplers. Environmental Monitoring and Assessment, 80(2): 149-173.

Carpenter, S.R., Caraco, N.F., Correll, D.L., Howarth, R.W., Sharpley, A.N. and Smith, V.H., 1998. Nonpoint pollution of surface waters with phosphorus and nitrogen. Ecological Applications, 8(3): 559-568.

Chuang, H., 2002. Water-monitoring apparatus with anchor. Patent US 6486786.

Clesceri, L.S., Greenberg, A.E. and Eaton, A.D., 1998. Standard Methods for the Examination of Water and Wastewater, 20th Edition. American Public Health Association, New York.

Cooter, W.S., 2004. Clean Water Act assessment processes in relation to changing US Environmental Protection Agency management strategies. Environmental Science & Technology, 38(20): 5265-5273.

Deletic, A., 1998. The first flush load of urban surface runoff. Water Research, 32(8): 2462-2470.

FDEP, 2006a. TMDL Report: Nutrient TMDL for Alachua Sink, WBID 2720A. Florida Department of Environmental Protection. Bureau of Watershed Management, Tallahassee, FL. http://www.dep.state.fl.us/water/tmdl/docs/tmdls/draft/alachuasinktmdl_edited_1_23_06.pdf.

FDEP, 2006b. TMDL Protocol. Florida Department of Environmental Protection. Task Assignment 00.303/05-003. Bureau of Watershed Management, Tallahassee, FL. http://www.dep.state.fl.us/water/tmdl/docs/TMDL_Protocol.pdf.

Glasgow, H.B., Burkholder, J.M., Reed, R.E., Lewitus, A.J. and Kleinman, J.E., 2004. Real-time remote monitoring of water quality: a review of current applications, and advancements in sensor, telemetry, and computing technologies. Journal of Experimental Marine Biology and Ecology, 300(1-2): 409-448.

Hatfield, K., Annable, M., Cho, J.H., Rao, P.S.C. and Klammler, H., 2004. A direct passive method for measuring water and contaminant fluxes in porous media. Journal of Contaminant Hydrology, 75(3-4): 155-181.

Hatfield, K., Rao, P.S.C., Annable, M.D. and Campbell, T.J., 2002. Device and method for measuring fluid and solute fluxes in flow systems. Patent US 6402547.

Hemmerling, E.M., 1964. Fundamentals of College Geometry. John Wiley & Sons, Inc., New York, 401 pp.

Herschey, R.W., 1985. Streamflow Measurement. Elsevier Science Publishing Co., New York, 553 pp.

Hornberger, G.M., Raffensperger, J.P., Wiberg, P.L. and Eshleman, K.N., 1998. Elements of Physical Hydrology. The Johns Hopkins University Press, Baltimore, 302 pp.

Inoue, M., Simunek, J., Shiozawa, S. and Hopmans, J.W., 2000. Simultaneous estimation of soil hydraulic and solute transport parameters from transient infiltration experiments. Advances in Water Resources, 23(7): 677-688.

ITRC, 2006. Technology Overview of Passive Sampler Technologies. Interstate Technology & Regulatory Council, Authoring Team, Washington, DC.

Jarvie, H.P., Withers, P.J.A. and Neal, C., 2002. Review of robust measurement of phosphorus in river water: sampling, storage, fractionation and sensitivity. Hydrology and Earth System Sciences, 6(1): 113-131.

Klammler, H., Hatfield, K., Annable, M., Jawitz, J.W. and Padowski, J.C., 2004. The passive surface water flux meter to measure cumulative water and solute mass fluxes. EOS Transactions, Fall Meeting Supplement, 85(47): Abstract H13C-0422.

Klammler, H., Newman, M.A., Szilagyi, E., Padowski, J.C., Hatfield, K., Jawitz, J.W. and Annable, M.D., 2007. Initial Test Results for a Passive Surface Water Flux Meter to Measure Cumulative Water and Solute Mass Fluxes. Environmental Science & Technology, 41(7): 2485-2490.

Kookana, R.S., Schuller, R.D. and Aylmore, L.A.G., 1993. Simulation of Simazine Transport through Soil Columns Using Time-Dependent Sorption Data Measured under Flow Conditions. Journal of Contaminant Hydrology, 14(2): 93-115.

Lee, J.H., Bang, K.W., Ketchum, L.H., Choe, J.S. and Yu, M.J., 2002. First flush analysis of urban storm runoff. Science of the Total Environment, 293(1-3): 163-175.

Li, L.Q., Yin, C.Q., He, Q.C. and Kong, L.L., 2007. First flush of storm runoff pollution from an urban catchment in China. Journal of Environmental Sciences-China, 19(3): 295-299.

Maraqa, M.A., 2001. Prediction of mass-transfer coefficient for solute transport in porous media. Journal of Contaminant Hydrology, 50(1-2): 1-19.

Maraqa, M.A., Wallace, R.B. and Voice, T.C., 1999. Effects of residence time and degree of water saturation on sorption nonequilibrium parameters. Journal of Contaminant Hydrology, 36(1-2): 53-72.

McManus, M.A., Alldredge, A.L., Barnard, A.H., Boss, E., Case, J.F., Cowles, T.J., Donaghay, P.L., Eisner, L.B., Gifford, D.J., Greenlaw, C.F., Herren, C.M., Holliday, D.V., Johnson, D., MacIntyre, S., McGehee, D.M., Osborn, T.R., Perry, M.J., Pieper, R.E., Rines, J.E.B., Smith, D.C., Sullivan, J.M., Talbot, M.K., Twardowski, M.S., Weidemann, A. and Zaneveld, J.R., 2003. Characteristics, distribution and persistence of thin layers over a 48 hour period. Marine Ecology-Progress Series, 261: 1-19.

Meybeck, M. and Helmer, R., 1989. The Quality of Rivers - from Pristine Stage to Global Pollution. Global and Planetary Change, 75(4): 283-309.

Milne-Thomson, L.M., 1960. Theoretical Hydrodynamics. The MacMillan Company, New York, 660 pp.

Montes, S., 1998. Hydraulics of Open Channel Flow. American Society of Civil Engineers Press, Reston, VA, 697 pp.

Nkedi-Kizza, P., Biggar, J.W., Selim, H.M., Vangenuchten, M.T., Wierenga, P.J., Davidson, J.M. and Nielsen, D.R., 1984. On the Equivalence of 2 Conceptual Models for Describing Ion-Exchange During Transport through an Aggregated Oxisol. Water Resources Research, 20(8): 1123-1130.

Padowski, J.C., 2005. Direct measurement of water and solute fluxes using a passive surface water flux meter. Master of Science Thesis, University of Florida, Gainesville, 67 pp.

Panno, S.V., Krapac, I.C. and Keefer, D.A., 1998. A new device for collecting time-integrated water samples from springs and surface water bodies. Environmental & Engineering Geoscience, 4(3): 375-383.

Parry, R., 1998. Agricultural phosphorus and water quality: A US Environmental Protection Agency perspective. Journal of Environmental Quality, 27(2): 258-261.

Petty, J.D., Huckins, J.N., Alvarez, D.A., Brumbaugh, W.G., Cranor, W.L., Gale, R.W., Rastall, A.C., Jones-Lepp, T.L., Leiker, T.J., Rostad, C.E. and Furlong, E.T., 2004. A holistic passive integrative sampling approach for assessing the presence and potential impacts of waterborne environmental contaminants. Chemosphere, 54(6): 695-705.

RPG, 2003. PlanEastGainesville Final Report. Renaissance Planning Group. Metropolitan Transportation Planning Organization for the Gainesville Urbanized Area, Gainesville, FL. http://www.planeastgainesville.org/downloads/Final/Ch4-SweetwaterBranch.pdf.

Selker, J.S. and Rupp, D.E., 2005. An environmentally driven time-integrating water sampler. Water Resources Research, 41(9).

Simunek, J., van Genuchten, M.T. and Sejna, M., 2005. The HYDRUS-1D Software Package for Simulating the Movement of Water, Heat, and Multiple Solutes in Variably Saturated Media, Version 3.0. HYDRUS Software Series 1. Department of Environmental Sciences, University of California Riverside, Riverside, CA.

SJRWMD, 2007. Hydrologic Data. St. Johns River Water Management District, Division of Hydrologic Data Services, Palatka, FL. http://arcimspub.sjrwmd.com/website/dahds/design/index.html.

Taebi, A. and Droste, R.L., 2004. First flush pollution load of urban stormwater runoff. Journal of Environmental Engineering and Science, 3(4): 301-309.

Tokhtuev, E., Skirda, A., Slobodyan, V. and Owen, C., 2005. Remote sampling system. In: U.S.P.a.T. Office (Editor). Apprise Technologies, Inc., United States of America.

USEPA, 1999. Protocol for Developing Nutrient TMDLs. United States Environmental Protection Agency. EPA 841-B-99-007. Office of Water, Washington, DC.

Vrana, B., Mills, G.A., Allan, I.J., Dominiak, E., Svensson, K., Knutsson, J., Morrison, G. and Greenwood, R., 2005. Passive sampling techniques for monitoring pollutants in water. Trends in Analytical Chemistry, 24(10): 845-868.

Waldon, M.G., 2004. Estimation of average stream velocity. Journal of Hydraulic Engineering-ASCE, 130(11): 1119-1122.

Ward, B., Wanninkhof, R., Minnett, P.J. and Head, M.J., 2004. SkinDeEP: A profiling instrument for upper-decameter sea surface measurements. Journal of Atmospheric and Oceanic Technology, 21(2): 207-222.

Worsfold, P.J., Gimbert, L.J., Mankasingh, U., Omaka, O.N., Hanrahan, G., Gardolinski, P., Haygarth, P.M., Turner, B.L., Keith-Roach, M.J. and McKelvie, I.D., 2005. Sampling, sample treatment and quality assurance issues for the determination of phosphorus species in natural waters and soils. Talanta, 66(2): 273-293.

BIOGRAPHICAL SKETCH

Erin C. Atkinson was born in Rochester, NY in 1982. Growing up, she spent summers with her family in the Thousand Islands of upstate New York. After graduating from Webster High School in 2000, she attended The University of Chicago to study earth sciences. Her coursework gave her the opportunity to travel to several interesting and diverse geological destinations including Montana, Nova Scotia, Mexico, Italy, and Iceland. As an undergraduate she also participated in summer research internships at the University of New Hampshire and NASA Goddard Space Flight Center. Erin earned a BS from the Department of Geophysical Sciences in June 2004, and remained in Hyde Park for an additional year, working as the manager of a paleoceanography lab.

In August 2005, Erin moved to Gainesville to pursue an MS in Soil and Water Science Departmentat the University of Florida. Highlights of her time spent in the Environmental Hydrology Lab include learning Darcy's Law, attending conferences in San Francisco and Acapulco, and witnessing the brutality of a storm event in Sweetwater Branch. She also thoroughly enjoyed the warm winters, southern barbeque, and alligators of the region.

After her August 2007 graduation, Erin is getting married in the Grenell Island Chapel and moving to San Salvador Island, Bahamas, where she will live and work at the Gerace Research Centre with her husband, Tom, and their dog, Zipper.